Final Report on NASA Contract NAG5-854

GODDARD GRANT

243108 IN-43-CR

P-73

An Investigation of Satellite Sounding Products for the Remote Sensing of the Surface Energy Balance and Soil Moisture

for the period of

1 October 1986 to 30 August 1989

submitted by

George R. Diak

Cooperative Institute for Meteorological Satellite Studies
(CIMSS)
Space Science and Engineering Center
University of Wisconsin-Madison
1225 West Dayton Street
Madison, WI 53706

November 1989

1. INTRODUCTION

Improved techniques for the remote sensing of the land surface energy balance (SEB) and soil moisture would greatly improve prediction of climate and weather as well as be of benefit to agriculture, hydrology and many associated fields. Most of the satellite remote sensing methods which have been researched to date rely upon satellite-measured infrared surface temperatures or their time changes as a remote sensing signal. Optimistically, only four or five levels of information (wet to dry) in surface heating/ evaporation are discernable by surface temperature methods and a good understanding of atmospheric conditions is necessary to bring them to this accuracy level.

In this work, we have researched skin temperature methods, as well as begun work on several new methods for the remote sensing of the SEB, some elements of which are applicable to current and retrospective data sources and some which will rely on instrumentation from the Earth Observing System (EOS) program in the 1990s.

2. RESEARCH ACCOMPLISHMENTS

A. Satellite Skin Temperatures and the SEB

Satellite-measured infrared land surface temperatures have been used by ourselves and by a number of other investigators to infer the surface turbulent flux balance and soil moisture. Generally, in these methods the surface temperature signal is coupled to a surface layer or Planetary Boundary Layer (PBL) model to estimate sensible heating and also evapotranspiration through energy balance considerations. If soil moisture is derived, additional parameterizations are required which relate the evapotranspiration to soil moisture. Early attempts at using remote surface temperature measurements for these purposes were hampered by inaccuracies in the surface temperatures and the use of low-level measurements of air temperature and wind speed (typically at anemometer height) as upper boundary conditions to calculate energy transfers. Inherent in these surface temperature methods is an evaluation of the surface-air temperature difference to estimate sensible heating. Assessing this gradient using surface-air temperature differences over short vertical distances means the resulting flux diagnosis is subject to large and unacceptable errors. Most recent work has attempted to mitigate these problems first by using measured surface temperature **changes** instead of absolute temperature measurements (to negate absolute temperature errors caused by errors in surface emissivity, sensor calibration, atmospheric corrections and other sources) and also effectively moving atmospheric boundary conditions upward in

the vertical using a planetary boundary layer model, so that the surface-air temperature gradient is evaluated over a larger vertical interval.

Recently, Diak and Stewart in work funded by this grant (henceforth DS, copy enclosed) have used satellite-measured surface temperature changes and a composite surface layer-mixed layer PBL model (MLM) to diagnose the sensible and latent heating at the land surface over large (continental United States) spatial scales. The mixed layer model (Fig. 1 in DS) was selected for its accuracy under conditions appropriate to SEB remote sensing (shortwave forcing at the surface and a growing PBL) and also because of its simplicity, which makes the physical model competitive with statistical techniques designed for the same purpose. Similar mixed layer formalisms have been shown to be extremely accurate in the prediction of PBL height and temperature by other investigators when measured surface fluxes are used to drive the model.

A series of 12-hour MLM simulations (12-00 UTC) are shown in Fig. 6 of DS, when satellite-measured surface temperatures at hourly intervals are used to force the model surface energetics (replacing net shortwave flux as forcing). As shown, driving the surface and PBL with these temperature changes, the soundings which resulted from the MLM show a good resemblance to the collocated radiosonde verification soundings at 00 UTC.

A product of this procedure is a diagnosis of the sensible heat flux at the surface and also of the latent heat flux through energy balance considerations. Figure 5 of DS shows an evaluation of sensible and latent heating derived in this manner across the sharp transition zone of surface moisture regimes in the central United States. While the spatial gradients shown in this figure are very reasonable, a complete error analysis from this DS study is only moderately encouraging for the use of surface temperatures in the diagnosis of the SEB. Table 3 of DS shows estimated errors in surface sensible heating using surface temperatures in the MLM (latent heating errors in this energy balance scheme are approximately equal, but of opposite sign). In this MLM-generated evaluation, representative errors in satellite-measured surface temperature change, surface roughness and atmospheric conditions have all been included in the model-evaluated surface energy budget. Results are shown in this table for a range of surface moisture and surface roughness climatologies.

The standard error in sensible heating is greater than 2 $MJ\text{-}m^{-2}$, which is about 10% of net incoming solar radiation at the surface on a summer day in mid-latitudes. Of special interest is the rapid increase of errors in the "smooth and

dry" regimes shown in this table. This error is due to the interaction of errors in the assignment of surface roughness character with errors in the measurement of surface temperature change. Here, small errors in designating surface characteristics make large differences in atmospheric transfers and model interpretation of surface temperature change in terms of the SEB. These general results are probably somewhat optimistic because of the simplicity of the surface model, which does not yet explicitly take into account differing canopy characteristics (leaf area index, biomass, ratio of vegetation/bare soil, etc.) which can also modify the temperature response of the surface for a given energy balance.

Thus, most of the errors in evaluating the SEB from satellite-measured surface temperatures come from the interaction of errors in characterizing the surface with errors in measurement of its temperature change. These errors span the range of PBL models from simple to complex. It is unlikely in the near future that translations of vegetation/land use information into quantitative surface indices will have the required accuracy to be of much help over the large spatial and temporal scales which the community needs to address in climate and weather studies.

In this investigation, however, it has become clear that satellite-measured surface temperatures are not the only remote sensing signal which can be exploited for SEB remote sensing purposes. Combinations of satellite surface temperature data and synoptic information have the potential to improve current and retrospective capabilities, while in the 1990s, several new satellite instruments may offer intriguing possibilities for improving SEB determination from space. In this research, we have begun preliminary investigations of several new remote sensing signals and techniques.

B. The PBL Height Excursion as a Remote Sensing Signal

The extremely strong dependence of the height excursion of the daytime PBL on the surface turbulent fluxes is a signal which we have begun to research for use in current and retrospective studies of the SEB. Figure 7 of DS shows the 12-hour ascent of mixed layer heights predicted in a series of MLM simulations for a variety of surface moisture and roughness conditions as a function of the 12-hour surface sensible heating total. The initial conditions used in this set of model simulations were from a specific synoptic station. Initializing the MLM with synoptic soundings with widely varying conditions in atmospheric temperature, moisture and wind speed, however, yielded similar results to that shown in this figure. Of importance here is that across this large range of values of surface

conditions and air masses there is a very strong relationship between mixed layer growth and surface heating. This is due to the fact that under conditions of surface heating the thermally induced buoyancy flux usually dominates other mechanisms of PBL growth, such as mechanical turbulence and wind shear across the top of the PBL. Similar observations for the growth of the marine boundary layer in a case study of a cold-air outbreak over the Gulf Stream have been made by Chou and Atlas (1982) who concluded that "the growth of the boundary layer and sensible heating may be used as proxies for one another."

The use of this signal of mixed layer growth (DELH) has possibilities for current observing systems which we have begun to investigate in this research and also for planned observing systems which we will be investigating under continued NASA support. In combination with satellite-measured surface temperatures, there is potential to gain insight into the SEB and also to derive some important information about the transfer characteristics of the surface, which will be important not only for remote sensing purposes, but also in the areas of numerical climate and weather prediction.

It can be seen in principle that with the measurements of the quantities DELH (the diurnal excursion of the PBL height) and DELTS (the diurnal surface temperature range from satellites) and expressing these two quantities in the following manner

$$DELH = F(Q_0, Z_0) \quad (1)$$

$$DELTS = G(Q_0, Z_0) \quad (2)$$

where

Q_0 = surface sensible heating

Z_0 = surface roughness

that we have two equations in two unknowns and it is possible to solve for not only the total surface sensible heating, Q_0, but also to say something about the surface roughness provided that suitable functional relationships for F and G can be determined.

Figure 2 of Diak (1989, henceforth DI, copy enclosed) is a graphical representation of this physical system derived from MLM simulations. Shown are isolines of the 12-hour rise of the PBL height and isolines of the 12-hour surface temperature range, versus both roughness height and surface energy balance (Bowen ratio), for two different surface moisture and roughness regimes. These results have

been generated by the MLM from specific radiosonde atmospheric states at 12 UTC and varying Z_0 and the Bowen ratio, B_0, around the climatological means for the two locations. It can be seen in this figure that for a specific DELTS,DELH measurement pair that the solution to Eqs. (1) and (2) for B_0 and Z_0 would be the intersection of the appropriate isolines and that here the functional relationships F and G have been successfully determined through MLM simulations from a base atmospheric state.

In DI, this technique was applied to a case study day (20 July 1981) to assess the surface energy balance and roughness height variations across the strong climatological transition zone of moisture and roughness in the central United States. Preliminary error statistics from this work (see DI) suggest that these techniques will yield a better evaluation of the SEB than would be possible using surface temperature data alone and that there will not be the large degradation of accuracy in the "smooth and dry" regimes as there is with surface temperature techniques. Lidar instrumentation proposed for the 1990's, which is planned to be able to measure the PBL height to an accuracy of 50m, will extend the use of such techniques to locations where synoptic data is not available. Another advantage of this methodology is that it will produce "effective" values of B_0 and Z_0, which by definition will yield the measurement values of DELH and DELTS in the model used for their derivation. As surface and PBL parameterizations grow more realistic and complete, the results of the techniques will converge towards values with increased physical meaning.

C. Satellite Atmospheric Radiances as a Remote Sensing Signal

Table 5 in DS shows simulated brightness temperatures (from a forward radiance model and 12-hour MLM forecast temperature changes) for several channels of the VISSR Atmospheric Sounder (VAS) instrument on board the current series of geostationary satellites. The channels shown receive thermal radiation from progressively lower regions of the atmosphere with increasing channel number. All the channels shown may detect radiation both from the lower atmosphere and surface. In this table, the surface temperature contribution to brightness temperature has been removed through knowledge of the surface temperature from the MLM. The changes in brightness temperatures with increasing surface sensible heating shown are then entirely from changes in the lower atmosphere induced by this heating. An advantage to using the atmospheric signal is that it is quasi-independent of surface type (roughness) and thus, in principle, is more easily interpreted in terms of the SEB than are surface skin temperatures. Unfortunately, the idealized signals which are shown in this table are only very marginally separable using the VAS instrument. First

of all, the channels displayed in this table have an instrument noise level of about .3K. Secondly, in practice it is only realistically possible to make the required correction for the surface temperature change in the total brightness temperature change to an accuracy of a few tenths of a degree.

The AIRS instrument proposed to be launched by NASA in the 1990s will make radiance measurements at a much finer spectral resolution (several thousand channels in the infrared, as opposed to 12 for the VAS) than do current instruments. Additionally, the High resolution Interferometer Sounder (HIS) instrument with similar capabilities developed at the CIMSS, is currently being studied by the National Oceanic and Atmospheric Administration (NOAA) as a replacement for the filter wheel radiometer instruments now slated for geostationary satellites to be flown in the 1990s. The fine spectral resolution of these new instruments will importantly offer more than a factor of two improvement in the vertical resolving power of the atmosphere over any current sounder. This will result in substantially larger atmospheric brightness temperature signals of the type shown in Table 5 of DS due to better resolution of the PBL.

As a part of this program (Masters thesis of C. J. Scheuer, henceforth CS, copy of abstract, introduction and selected tables enclosed), we began a preliminary investigation on the use of the high-spectral resolution information from instruments such as the HIS and AIRS to measure the SEB. Since neither the real satellite data nor the SEB measurements over the wide range of surface regimes necessary for such an evaluation yet exist, it was necessary to perform this study as a simulation experiment.

In this study, a PBL model (the MLM described in previous sections) was employed to generate a set of atmospheric profiles where the lower to mid-troposphere was modified by surface forcings representing a variety of SEB conditions. HIS transmittances for the model initialization and output from later times in the MLM integration were calculated using a regression scheme based on a line-by-line transmittance database and time differences of radiances were constructed. Three different radiance signatures were investigated. The first two are based on 12 and 8 hour PBL model integration intervals and include only the time difference in the atmospheric term of the Radiative Transfer Equation (RTE). The third was based on eight hour PBL model runs and included both atmospheric and surface term (e.g., surface temperature contribution term) of the RTE.

Subsequently, an eigenvector analysis on the simulated radiance difference signals and a regression analysis on the surface energy terms which came from the model integrations

was performed. The purpose of this analysis was to provide insight as to how the simulated time changes of radiances in the three signals related to the SEB and restructuring of the lower atmosphere.

A summary of the model surface energy balance constituents which were regressed against the eigenvector coefficients from the decomposition of the radiance change signals are shown in Table 5 of CS. Table 6 of CS provides statistics from the multiple linear regression analysis of these SEB quantities against the eigenvector coefficients of the 12-hour atmospheric radiance change signal. This signal had the best results of the three signals previously delineated. Importantly for SEB determination, the correlation values for surface sensible and latent heating values are quite good.

The results of this eigenvector decomposition and statistical analysis were subsequently applied to examine a small independent data set. Forward HIS radiances were calculated at 1200 and the following 0000 UTC for the atmospheric soundings from three radiosonde location. Time differences of the three sets of atmospheric spectra were made and the results of the eigenvector and regression analyses in the dependent data set were used to predict the SEB quantities at the three locations. Unfortunately, no measurement surface flux values existed at these locations for a direct comparison. Comparisons were made, however, with the flux results obtained for the same stations using surface temperatures to estimate the flux balance (in the DS study) and with climatology. Tables 11-13 of CS show this comparison. In these tables, "retrieval" indicates results obtained from the HIS spectra, while "model" refers to the estimations made using surface temperatures in the MLM. While this study of atmospheric radiances to diagnose the SEB is very preliminary, the results obtained encourage us to pursue the technique in ongoing work.

3. CONCLUSIONS

In this research, we have investigated the utility of several remotely sensed and in-situ signals for the evaluation of the land surface energy balance. These data are the surface skin temperature remotely sensed from satellites, the diurnal rise of the planetary boundary layer height from radiosonde reports and the diurnal change of atmospheric radiances from the VAS and HIS.

Especially in combination, these data sources have the potential to expand current capabilities for monitoring and numerical modelling of the SEB. Current research has identified these SEB signals and provided preliminary indications of how they may be utilized. To be of more than

academic value, however, it is necessary that follow-up investigations refine the techniques described here and also, importantly, establish at least a basic operational framework to take advantage of these measurements of the SEB. A remote sensing system can be envisioned for land surface processes where the remote sensing system and an analysis/forecast model are used in a complementary manner, similar to the four-dimensional data assimilation systems which are now being researched heavily for numerical weather prediction purposes. It will be the goal of our ongoing NASA-sponsored research to refine the SEB measurement techniques described here, as well as develop the guidelines for this type of assimilation system.

REFERENCES

Chou, S., and D. Atlas, 1982: Satellite estimates of ocean-air heat fluxes during cold air outbreaks. Mon. Wea. Rev., 110, 1434-1450.

Diak, G. R., and T. R. Stewart, 1989: Assessment of surface turbulent fluxes using geostationary satellite surface skin temperatures and a mixed layer planetary boundary layer scheme. J. Geophys. Res., 94, 6357-6373.*

Diak, G. R., 1989: Evaluation of heat flux, moisture flux and aerodynamic roughness at the land surface from knowledge of the PBL height and satellite-derived skin temperatures. Accepted for publication in J. Agricultural and Forest Meteorology.*

Scheuer, C. J., 1989: The utility of the high resolution interferometer sounder in the remote sensing of land surface energetics and planetary boundary layer development. Masters thesis, Department of Meteorology, University of Wisconsin-Madison, 82pp.*

*Indicates partial or complete copy included in Appendix A.

APPENDIX A

Publications from NASA Grant NAG5-854

JOURNAL OF GEOPHYSICAL RESEARCH, VOL. 94, NO. D5, PAGES 6357-6373, MAY 20, 1989

ASSESSMENT OF SURFACE TURBULENT FLUXES USING GEOSTATIONARY SATELLITE SURFACE SKIN TEMPERATURES AND A MIXED LAYER PLANETARY BOUNDARY LAYER SCHEME

George R. Diak and Tod R. Stewart

Cooperative Institute for Meteorological Satellite Studies
Madison, Wisconsin

Abstract. A method is presented for evaluating the fluxes of sensible and latent heating at the land surface, using satellite-measured surface temperature changes in a composite surface layer-mixed layer representation of the planetary boundary layer. The basic prognostic model is tested by comparison with synoptic station information at sites where surface evaporation climatology is well known. The remote sensing version of the model, using satellite-measured surface temperature changes, is then used to quantify the sharp spatial gradient in surface heating/evaporation across the central United States. An error analysis indicates that perhaps five levels of evaporation are recognizable by these methods and that the chief cause of error is the interaction of errors in the measurement of surface temperature change with errors in the assignment of surface roughness character. Finally, two new potential methods for remote sensing of the land-surface energy balance are suggested which will rely on space-borne instrumentation planned for the 1990's.

1. Introduction

One of the most difficult tasks in modeling and monitoring of the Earth's surface and atmosphere is the specification of the fluxes of heat, momentum, and moisture at the land surface. These fluxes are influenced by the input radiation, soil moisture and other soil properties, surface albedo, vegetation character, atmospheric conditions, and a host of other related variables. Modeling the exchanges at the air-soil interface over the space and time scales inherent in climate and weather models is not yet possible in a totally rigorous manner, owing to the complexities of the physical systems involved. Many parameterization schemes have thus been developed over the years, at steadily increasing levels of sophistication, to predict land surface exchanges.

Some useful information has been gained through global assessment of vegetation regimes, albedos, and other surface characteristics from land use information and/or satellite data surveys (see, for example, Hummel and Reck [1979]; Matthews [1984]; Kung et al. [1964]). A general research goal remains the translation of land use and vegetation information into quantitative indices which yield accurate flux predictions when used in climate and weather models (see, for example, Sellers et al. [1986]). The effects of errors in the calculation of surface evaporation on climate simulations has been discussed by Kasahara and Washington [1971], Suarez et al. [1983], and many others. For shorter-term forecasting, evidence is also accumulating [Diak et al., 1986, henceforth DHB; Benjamin and Carlson, 1986; Yan and Anthes, 1988] that accurate surface flux predictions may be important for the accurate prediction of synoptic and mesoscale events and especially forecasts of precipitation processes. These studies suggest that deviations from climatological values of surface conditions, which cannot be described by the climatological data sets, may warrant investigation.

Satellite remote-sensing methods are currently offering some insights in diagnosis and modeling of the surface energy balance and may be useful both in establishing a link between qualitative information and fluxes and in monitoring turbulent and radiative fluxes at the surface over various time scales.

Several approaches have been developed in the last decade for the remote sensing of the surface energy balance and soil moisture. Microwave techniques [Schmugge et al., 1980] have the potential to allow direct sensing of the soil water content via the effects of moisture on soil dielectric properties. Separating the effects of vegetation in the microwave signal remains a problem, as does the translation of volumetric soil water information into information which can be used by soil canopy models to predict surface exchanges.

Satellite-measured infrared land surface temperatures have been used by a number of investigators [Price, 1982; Wetzel et al., 1984; Carlson et al., 1981; Taconet et al., 1986] to infer the surface turbulent flux balance and soil moisture. Generally, in these methods the surface temperature signal is coupled to a surface layer or planetary boundary layer (PBL) model to estimate sensible heating and evapotranspiration through energy balance considerations. If soil moisture is derived, additional parameterizations are required which relate the evapotranspiration to soil moisture. Early attempts at using remote surface temperature measurements (see, for example, Kanemasu et al. [1976] for these purposes were hampered by inaccuracies in the temperatures and the use of low-level measurements of air temperature and wind speed (typically at anemometer height) as upper boundary conditions to calculate energy transfers. Inherent in these surface temperature methods is an evaluation of the surface-air temperature difference to

Paper number 89JD00179.
0148-0227/89/89JD-00179$05.00

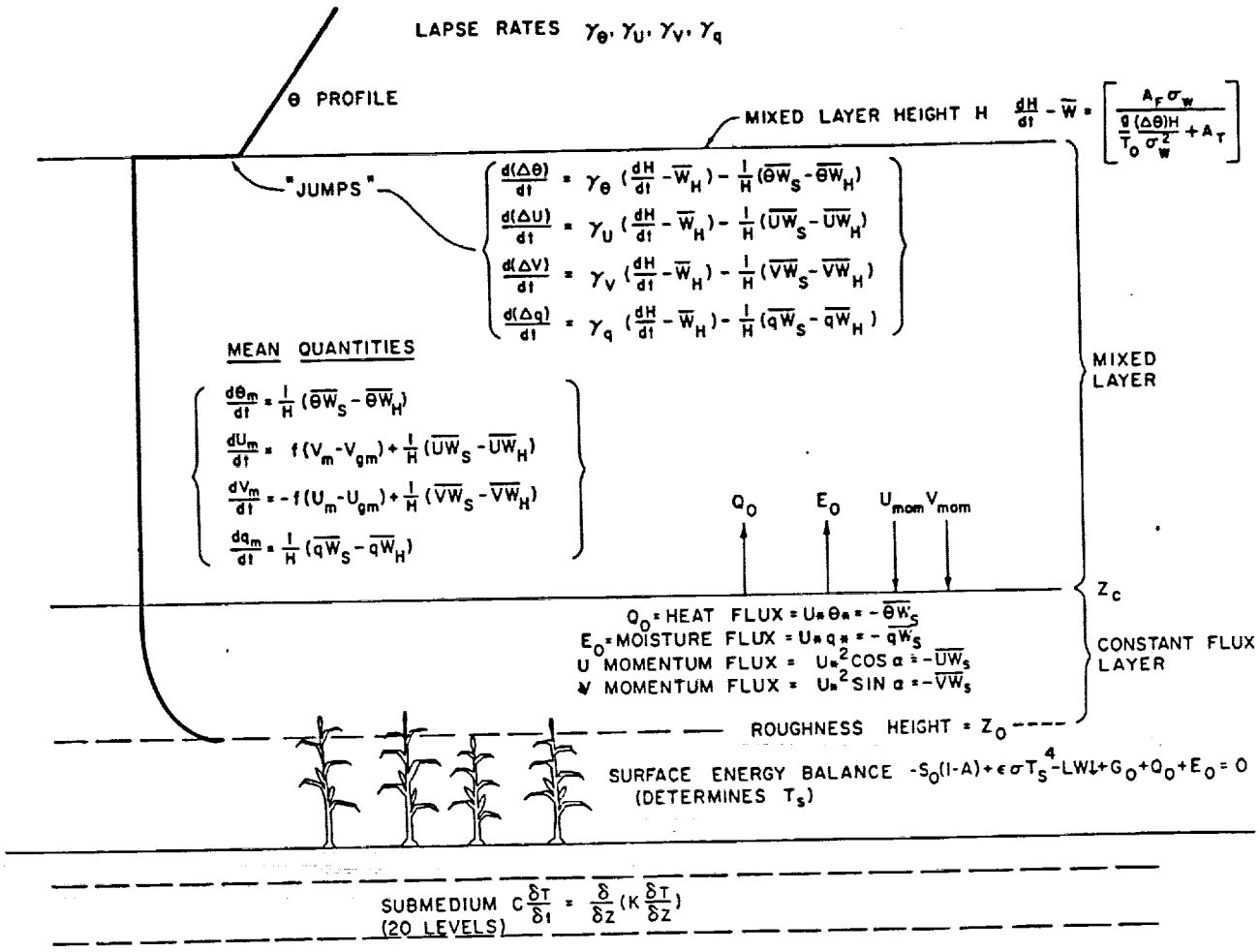

Fig. 1. Pictorial representation of hybrid mixed layer-surface layer model.

evaluate sensible heating. Assessing this gradient using surface-air temperature differences over short vertical distances, the resulting flux diagnosis is subject to large and unacceptable errors. More recent work has attempted to mitigate these problems (1) by using measured surface temperature changes instead of absolute temperature measurements (to negate absolute temperature errors caused by errors in surface emissivity, sensor calibration, atmospheric corrections, and other sources) and (2) by also effectively moving atmospheric boundary conditions upward in the vertical, using a PBL model, so that the surface-air temperature gradient is evaluated over a larger vertical interval.

2. Application of a Mixed Layer Model to Surface Remote Sensing

Mixed layer models (MLM) have been research tools for the study of the PBL for more than 20 years and have gone through several generations of improvements since their inception. Recent descriptions of these models and tests of their performance are given by Driedonks [1982a], Boers et al. [1984], Driedonks and Tennekes [1984], and others. The success of the models and their characteristics brought to our attention their potential value as a remote-sensing tool, when coupled to satellite-measured surface temperatures. The purpose of this paper is (1) to investigate the sensitivity of a MLM to changes in the surface energy balance and other surface characteristics, (2) to investigate the feasibility of using the MLM to diagnose the surface turbulent fluxes with the forcing of measured surface temperature changes, and (3) to assess how errors in measurement and in initial and boundary conditions influence the accuracy of this surface flux evaluation.

2.1. Model Description

The characteristics of mixed layer models (MLMs) have been discussed by many authors. We have borrowed heavily from excellent discussions by Driedonks and Tennekes [1984] and Driedonks [1982a] in this short description.

The observed structure of the mixed layer leads to so-called slab or jump models, where the vertical distribution of potential temperature, momentum, and mixing ratio are taken as independent of height and, at the top, a "jump" in these variables indicates a transition to the stable air above. The structure of our MLM is shown in Figure 1. Also shown are the surface and surface

layer model components, which will be described later.

Using the Boussinesq approximation and neglecting advection and condensation processes, conservation equations for mixed layer mean quantities and jumps are [Driedonks, 1982a]

$$\frac{dU_m}{dt} = f(V_m - V_{gm}) + 1/H\ (\overline{UW}_s - \overline{UW}_H) \quad (1)$$

$$\frac{dV_m}{dt} = -f(U_m - U_{gm}) + 1/H\ (\overline{VW}_s - \overline{VW}_H) \quad (2)$$

$$\frac{d\theta_m}{dt} = 1/H\ (\overline{\theta W}_s - \overline{\theta W}_H) \quad (3)$$

$$\frac{dq_m}{dt} = 1/H\ (\overline{qW}_s - \overline{qW}_H) \quad (4)$$

$$\frac{d(\Delta U)}{dt} = \gamma_u\ (dH/dt - \overline{W}_H) - 1/H\ (\overline{UW}_s - \overline{UW}_H) \quad (5)$$

$$\frac{d(\Delta V)}{dt} = \gamma_v\ (dH/dt - \overline{W}_H) - 1/H\ (\overline{VW}_s - \overline{VW}_H) \quad (6)$$

$$\frac{d(\Delta\theta)}{dt} = \gamma_\theta\ (dH/dt - \overline{W}_H) - 1/H\ (\overline{\theta W}_s - \overline{\theta W}_H) \quad (7)$$

$$\frac{d(\Delta q)}{dt} = \gamma_q\ (dH/dt - \overline{W}_H) - 1/H\ (\overline{qW}_s - \overline{qW}_H) \quad (8)$$

where

U, V	horizontal wind velocities;
θ	potential temperature;
q	mixing ratio;
H	mixed layer height;
$\overline{W}_H$	vertical velocity at mixed layer height;
$\gamma_{u,v,\theta,q}$	vertical gradients of winds, potential temperature and moisture above H;
f	coriolis acceleration;
t	time;
Δ	jump at the top of the mixed layer.

Other subscripts are

m	mean through mixed layer;
g	geostrophic;
s	evaluated at mixed layer base;
H	evaluated at mixed layer height H.

It is of note that the geostrophic terms have been dropped from the calculation of the U and V jumps (equations (5)-(6)), similar to Driedonks [1982a]. These terms allow an inertial oscillation in ΔU and ΔV, whose magnitude is a function of the initial conditions in these variables, which are generally not well determined from measurements.

The flux boundary conditions at Z=H ($-\overline{UW}_H$, etc.) may be taken to be

$$-\overline{\Phi W}_H = \Delta\Phi(dH/dt - \overline{W}_H) \quad (9)$$

for any variable Φ. In the example of heat flux ($\Phi=\theta$), this equivalence is derived recognizing that the mixed layer entrains an amount of heat proportional to $\Delta\theta$ times $(dH-\overline{W}_H)$ if the inversion base rises by $(dH-\overline{W}_H)$. Similar arguments hold true for momentum and moisture fluxes.

Closure of this set of equations requires specification of the fluxes of heat, momentum, and moisture at the base of the mixed layer and a choice of the formalism to specify dH/dt, the change of the mixed layer height with time. For dH/dt most researchers have based closure on the turbulent kinetic energy budget at the mixed layer height. A hierarchy of closure models has been developed considering various terms in this budget equation. We have selected a model proposed by Zilitinkevich [1975], which includes entrainment at the top of the mixed layer and the storage term in this equation to yield

$$\frac{dH}{dt} - W_H = \frac{A_F\sigma_w}{g/T_o[(\Delta\theta)H/\sigma_w^2] + A_T} \quad (10)$$

where

A_F, A_T	scaling constants (0.2, 1.5);
g	gravitational acceleration;
T_o	scaling temperature;
σ_w	scaling velocity for vertical component of turbulent kinetic energy.

Somewhat more sophisticated closure schemes exist which account for additional terms in the kinetic energy budget equation. Notably, in this formulation the contribution to entrainment of the vertical wind shear across the inversion has been neglected. In tests by Driedonks [1982a], inclusion of this term did not, in general, result in improved mixed layer predictions.

Descriptively then, MLMs predict through conservation relations the evolution of layer mean quantities, jumps at the top of the mixed layer, and the mixed layer height. Mean quantities change value through the difference between the fluxes at the mixed layer base and corresponding fluxes at H, which are realized through mixed layer growth and resulting entrainment processes. The growth of the mixed layer is fueled primarily by the production of buoyant kinetic energy generated by surface heating and also by mechanical turbulence generated by the surface momentum flux. The time change of jump quantities reflects the balance between surface fluxes and the entrainment rate and the vertical gradients in the air above Z=H.

2.2. Surface, Submedium, and Surface Layer

As previously described, the MLM requires a specification of fluxes at its base for closure of energy, momentum, and moisture equations. In model evaluations by other researchers, these have been generally specified through measurements. For model sensitivity tests they may be arbitrarily specified. In remote-sensing applications, with surface temperature as the input,

added relationships are necessary to calculate those fluxes from the surface temperature and properties of the mixed layer air. For this purpose, we have added a surface and constant-flux-type surface layer model to the MLM, as shown in Figure 1. These models are standard and are very similar to those described by DHB. Monin-Obukov scaling relationships are used to tum, heat, and moisture, with the particular forms from Businger et al. [1971]. Surface roughness height (Z_0) describes the surface aerodynamic transfer characteristic.

The depth of the constant-flux layer is allowed to vary in time in a similar manner to that of Deardorff [1972]; that is

$$Z_c = 0.025\ H \tag{11}$$

where Z_c is the height of the constant-flux layer above the Earth's surface. While Deardorff computes normalized differences between mixed layer means and values of prognostic variables at Z_c from Monin-Obukov scaling relationships, for the present our formulation assigns the values of these variables at Z_c as the mixed layer means. Stability in the surface layer scaling relationships is determined from the vertical gradient of virtual potential temperature (θ_v) between the surface and the height Z_c.

Either moisture availability (MA) or a Bowen ratio (B_0) can be used to describe the surface moisture character in model prognoses. Moisture availability is defined as the ratio of actual evaporation to potential evaporation, and thus in the model surface evaporation is determined by the relationship

$$E_0 = E_p MA \tag{12}$$

where E_p is determined in the surface layer relationships by

$$E_p = \rho_a\ L\ (q_s(T_s) - q_c)\ /\ R \tag{13}$$

and

E_0 latent heat flux;
E_p potential latent heat flux;
ρ_a air density;
L latent heat of evaporation;
$q_s(T_s)$ saturation mixing ratio at surface temperature T_s;
q_c mixing ratio at surface layer height Z_c;
R aerodynamic resistance for vapor transfer from surface layer relationships.

Alternatively, a Bowen ratio (B_0), defined as the ratio of sensible to latent heat flux, may be used to specify surface evaporation by the relationship

$$E_0 = Q_0/B_0 \tag{14}$$

where Q_0 is equal to sensible heat flux.

A difference between this model and DHB is in the treatment of the submedium, which is now done explicitly through application of the Fourier heat transfer equation at 20 levels, rather than the previous bulk soil flux method. That is

$$C\ \frac{\partial T}{\partial t} = \frac{\partial}{\partial Z}\left(K\ \frac{\partial T}{\partial Z}\right) \tag{15}$$

where

C soil volumetric heat capacity;
K thermal conductivity;
T soil temperature;
Z depth below surface.

Presently, C and K are kept at a constant median value for soils, and no similar formalism to (11) for soil moisture transfer is included. This 20-level formulation was chosen because of its availability in coded form, but it really is overkill compared to the sophistication of the rest of the model. A few brief intercomparisons showed that a soil model with four layers (Z=1, 5, 10, 20 cm) yielded soil fluxes which were usually within about 10% of the more detailed subsurface treatment.

The surface temperature change is evaluated through energy budget considerations.

$$-\ S_0\ (1-A) + \epsilon\sigma T_s^4 - LW\downarrow + G_0 + Q_0 + E_0 = 0 \tag{16}$$

where

S_0 incident solar flux;
A surface albedo;
ϵ surface emissivity;
σ Stefan-Boltzmann constant;
$LW\downarrow$ atmospheric longwave flux to the surface;
G_0 submedium flux.

The incident solar flux at the surface is computed using a simple clear-air model from Diak and Gautier [1983]. Atmospheric longwave flux to the surface is computed as a function of the surface layer air temperature and humidity, using the formulation of Lettau and Lettau [1978]. Currently, no longwave cooling of the atmosphere is included.

In the full prognostic mode (mode A) of running the MLM, the surface temperature is predicted from the surface flux balance. The surface moisture parameter (either MA or B_0) is specified, and this determines the partitioning of the available energy between primarily latent and sensible heating terms. In the remote-sensing mode (mode B) the time change of surface temperature is specified from satellite measurements, and it is this signal which drives the surface fluxes, rather than solar forcing. The solar forcing is still computed, however, and the latent heat flux is then derived as a residual in the surface energy balance after all of the other terms have been computed in the usual manner. Neither MA or B_0 are used explicitly in this remote-sensing mode, but rather are diagnostic quantities, which can be derived from the model fluxes or other output.

2.3. The Choice of a Mixed-Layer Model

It is appropriate here to explain the reasons behind the choice of this type of model for remote-sensing applications. Foremost among

these is the accuracy and simplicity of the MLM under conditions where the mixed layer develops owing to surface solar heating. It is exactly these types of conditions which are required to have a "signal" for infrared remote sensing, that is, rapidly changing surface temperatures and energy input into the system. Other researchers [Wetzel et al., 1984] have thus favored midmorning observation windows, when surface changes are maximized.

The mixed layer formalisms chosen here have been shown to be very accurate in the prediction of the evolution of the mixed layer. With surface heat flux specified from measurements, other mixed layer modelers have reported standard prediction errors of only several tenths of a degree in mixed layer temperature and less than 50 m in mixed layer height. The efficiency of the model makes it easy to run large numbers of tests and makes this model competitive with statistical methods. Model simplicity is helpful in gaining physical insight into the sensitivity of the prediction of PBL characteristics and surface fluxes to measurement and modeling errors.

Under certain simplified conditions the mixed layer equations can be integrated explicitly in time for sensitivity and error analysis. Such an investigation has been performed by Driedonks [1982b], which demonstrated other useful properties of these types of models for remote sensing applications. Conclusions from this study were that mixed layer time evolution is most sensitive to the surface heat flux and that the importance of the initial conditions decays very rapidly with mixed layer growth. In later sections of this paper, we will add some physical insight as to why this is so. Finally, important to energy remote-sensing schemes, MLMs conserve heat, momentum, and moisture.

3. Model Tests

3.1. Site Selection

The important points when considering the use of such models for remote-sensing applications are the possible consequences imposed by the use of parameterized surface fluxes to drive the model, rather than those which are measured and the effects of both potential errors of surface temperature excursion measurements and initial and boundary conditions on the model prediction.

Model test simulations were run for a total sample of eight sites for the day of July 20, 1981. This day has been investigated by DHB in a study of the effects of boundary layer processes on limited area forecasts and by several other groups [Smith et al., 1982; Peterson et al., 1983] because of the intense tornado episode which occurred in the Midwest late in the day.

The day was one of intense contrasts in soil moisture conditions across the continental United States. The antecedent precipitation index (API) is considered to be the best ground truth approximation to area-average soil moisture available on a routine basis over large areas [Wetzel et al., 1984]. The API for day i is calculated from the expression

$$API_i = P24_i + K(API_{i-1}) \quad (17)$$

P24 is the 24-hour precipitation total on day i, and K is a depletion constant. Our calculation of API for the 30 days preceding July 20 showed extremely dry conditions (API close to 0) westward to the California border from a north-south line extending from central North Dakota through the Texas panhandle. Most areas east of this line had API values closer to climatology.

For these model tests, our model was initialized using 1200 UTC radiosonde reports. Sites were limited to the areas where surface evaporation was relatively well known from the rainfall history and from vegetation climatology. In the tests we have chosen to use the Bowen ratio as the surface moisture parameter rather than moisture availability. Both of these parameters are simplifications in our model, since real evapotranspiration depends on a complex interaction between soil hydrology, plant physiology, solar energy input to the system, and atmospheric conditions. Research by Nappo [1975] has shown a relative insensitivity of model evaporation to changes in MA for values of MA around 0.5. In our own investigations (DHB), we have seen a hypersensitivity of model-predicted evaporation to MA in the dry range of MA values (0-0.1) which is situation-dependent and probably model-dependent. These facts made it difficult to select a "climatological" value of MA to use in these model tests and dictated the choice of the Bowen ratio.

Stations in western states constituted the "dry" sample, where surface Bowen ratio (B_0) was set to 1000 (essentially zero evaporation). Stations in the southern and Gulf states, which are climatologically the wettest areas in the continental United States, constituted the "wet" sample. Here B_0 was set to 0.4, an average of values researched from Sellers [1965], Oke [1978], and Bryson and Hare [1974] for this vegetation and rainfall climatology.

Albedo values for the sites were selected from Matthews [1984]. Roughness heights (Z_0) were chosen on the basis of land use and vegetation climatology. Surface emissivities (ϵ) for the different surface types were also varied, according to surface types, based on research by Kondrat'yev [1969], Fuchs and Tanner [1966], Taylor [1979], and Buettner and Kern [1965].

Since MLMs do not generally include advective processes, it was also important that advection not be large at the test sites. Temperature advection over 12 hours was evaluated using a limited area model run and was found to be small (<0.5°K) for the selected sites. It was required that the locations be mostly cloud-free over the course of the day, so that the model calculation of clear-air incident shortwave flux would be representative. Some of the wet sites developed small cumulus cloud cover during the day, not enough to significantly influence isolation, but enough to contaminate satellite surface temperature data [see Smith et al., 1970] and dictate the choice of alternate sites for later satellite data experiments.

This investigation represents a more difficult testing ground for the MLM than those reported in most other investigations for a

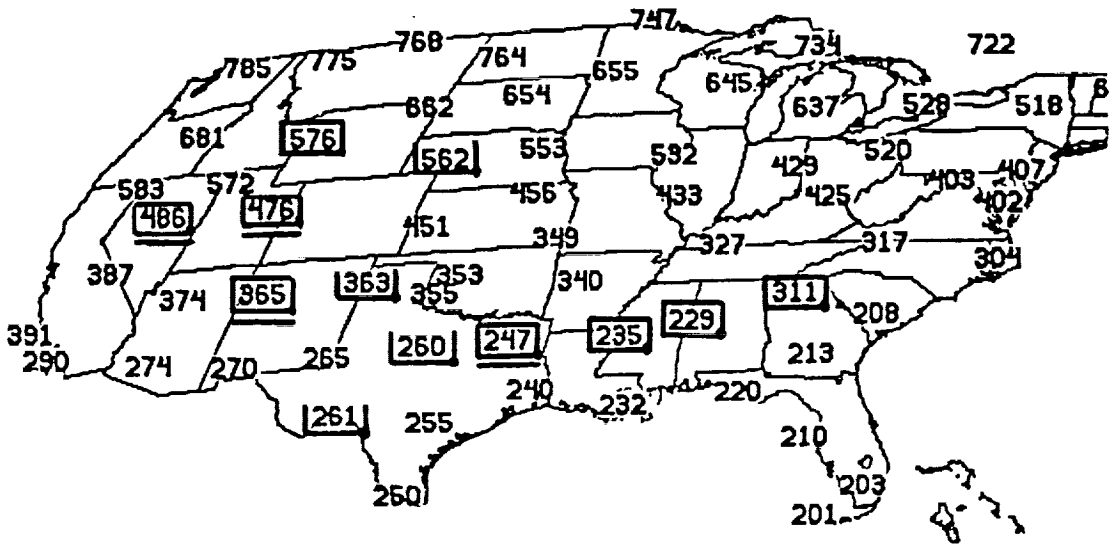

Fig. 2. Stations selected for model tests and satellite data experiments (WMO designations). A closed box around a station indicates a model test location, an open box shows a satellite data experiment site, and a closed box with an underline shows stations used for both experiment sets.

number of reasons: surface fluxes are parameterized rather than measured, the integration time of 12 hours is longer than has been considered in most other studies, and the dry samples represent an extreme in surface sensible heat flux that has not often been investigated. The net result is that while other researchers have generally reported mixed layer growth maxima of the order of 1000 m for shorter periods and wetter regimes, our dry samples have mixed layer growths which are typically 3 times this value.

Site locations for these experiments and later satellite data experiments are shown in Figure 2, and their characteristics are detailed in Table 1.

3.2. Model Initialization

Initial inversion heights (H) were diagnosed from mandatory and significant level information in the synoptic reports of 1200 UTC at the station locations. The initial values of the mixed layer potential temperature (θ_m) and potential temperature jump ($\Delta\theta$) were derived through a procedure suggested by Driedonks [1982a] which involves extrapolating the θ lapse above the mixed layer to the surface and subsequently calculating θ_m and $\Delta\theta$ to conserve the deficit between the extrapolated values and the actual sounding. Initialization of winds and mixing ratio was done somewhat differently, owing

TABLE 1. Station Characteristics for Model Tests and Satellite Experiments

STN	Character	Z_0,cm	A,%	ϵ,%	Test	Sat
365	dry	1	17	0.94	X	X
486	dry	1	20	0.94	X	X
476	dry	1	18	0.94	X	X
576	dry	1	18	0.94	X	X
235	wet	50	18	0.98	X	
247	wet	25	19	0.98	X	X
229	wet	50	18	0.98	X	
311	wet	50	18	0.98	X	
260	intermediate	5	19	0.96		X
261	intermediate	5	20	0.96		X
363	intermediate	5	19	0.96		X
562	intermediate	5	18	0.96		X

Shown are evaporation regime, roughness height (Z_0), albedo (A), and emissivity (ϵ). A cross in the "Test" column signifies that the station was used in a model test, while one in the "Sat" column indicates that the station was used in the satellite experiment set.

TABLE 2. Results of 12-hour Model Tests at Dry and Wet Station Locations

STN	Character	$\lvert\overline{\Delta T}\rvert$, °K	$\lvert\overline{\Delta V}\rvert$, m s^{-1}		T_{sm}, °K	T_{sp}, °K	$\lvert\Delta H\rvert$, mbar
			U	L			
365	dry	1.3	2.0	1.8	31.0	34.5	30
486	dry	.3	2.4	1.0	30.5	31.9	10
476	dry	2.2	2.3	0.4	28.5	30.6	10
576	dry	2.5	1.1	0.7	28.0	30.8	75
235	wet	2.9	0.3	0.9	4.5*	7.6	25
247	wet	0.7	0.8	0.3	7.0	6.6	15
229	wet	1.7	1.5	0.2	4.0*	6.7	5
311	wet	2.0	3.1	0.5	6.5*	7.1	10
$\bar{E}$ DRY		1.6	1.9	1.0			31
$\bar{E}$ WET		1.8	1.4	0.5			14
E TOT		1.7	1.7	0.7			22

Shown for each station are average temperature error magnitude, model versus radiosonde through the depth of the mixed layer ($\lvert\overline{\Delta T}\rvert$), wind error divided into partitions for the upper and lower half of the mixed layer ($\lvert\overline{\Delta V}\rvert$), the model-predicted and satellite-measured surface temperature excursions (T_{sp} and T_{sm}), and the error in model-predicted mixed layer height (ΔH). Average error ($\bar{E}$) for dry, wet, and total samples is also given.

* Indicates small cumulus cloud contamination.

to difficulties encountered extrapolating these quantities, which may exhibit large variations in the vertical. For U_m, V_m, and q_m, pressure-interval-weighted means were constructed, using sounding data below the inversion height. The jumps ΔU, ΔV, and Δq were then evaluated by differencing the mean values from those at the inversion height.

Values of the variables at the surface layer height were initialized at the mixed layer means. The surface temperature (T_s) was initialized with the radiosonde measurement of surface air temperature and subsoil temperatures were initialized with the previous day's average air temperature from hourly station reports.

Mean geostrophic winds (U_{gm}, V_{gm}) were initialized with the measured winds at the level immediately above the inversion height. As the mixed layer deepened through the simulation, they were updated with pressure-interval-weighted averages of the initial sounding winds over the depth of the mixed layer (excluding the levels below the initial mixed layer height). The assumption (albeit crude) is that these initial winds above the mixed layer represent the geostrophic balance. Fortunately, with any reasonable mixed layer growth the effects of these geostrophic terms on wind speeds are negligible compared to entrainment and surface friction.

3.3 Results

The 12-hour model runs were made between synoptic times (1200-0000 UTC) and evaluated by comparison with synoptic soundings at the final time. Table 2 shows model prediction versus verification statistics for the entire sample and also broken into several subcategories. The model results were encouraging to us in looking at the quantities which are important in the surface remote-sensing work. Model predictions of potential temperature (θ_m) and winds (U_m, V_m) are very important, as they will constitute the significant atmospheric boundary conditions when satellite-measured surface temperature changes are used to force the model. The average temperature of the mixed layer is well predicted for these model runs, as shown in Table 2, with an average error of 1.7°K. The largest error is exhibited at station 235 for the wet sample at 2.9°K. Temperature error is larger for the wet sample than for the dry. This is no surprise, since there is a larger uncertainty in specifying a Bowen ratio (and resulting surface turbulent flux balance) in wet areas than in the dry regions, where climatology and the rainfall history dictated negligible evaporation. As previously mentioned, other investigators using measured surface fluxes have been able to predict mixed layer temperatures to about 0.3°K accuracy. Our mean error of 1.7°K seems very reasonable, considering that it includes the effects of all the errors in specifying solar forcing, upper boundary conditions, surface parameters (albedo, Z_0, B_0, ϵ), and surface flux errors due to these errors, to other errors, and to simplifications in the parameterizations.

The mixed layer wind speed is also generally well-predicted. Verification wind speeds showed more variation in the vertical than did temperature and, of course, more than the model, since the MLM predicts a single mean wind speed for the depth of the mixed layer. Looking at Table 2, we see that model-generated winds verified best in the lower half of the mixed layer. This is fortunate, since lower level winds are what influence the turbulent transfers at the surface.

The predicted surface temperature change (maximum-minimum) is as important for remote-sensing purposes as is the prediction of

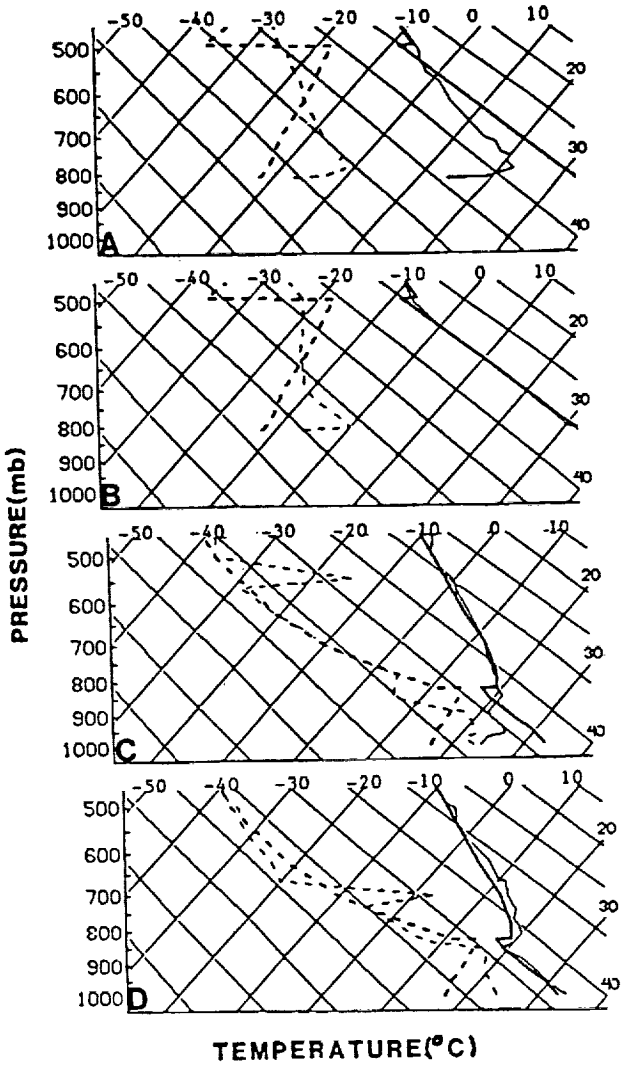

Fig. 3. Skew T - log p diagram of temperature and dew-point temperature (in degrees Celsius) versus pressure (in mbar) from "best" 12-hour MLM forecasts versus initial 1200 UTC conditions (Figures 3a and 3c) and 0000 UTC verification (Figures 3b and 3d). Dry and wet results are from stations 486 and 247, respectively. The dark and light lines are model prediction and radiosonde soundings, respectively.

atmospheric temperature and wind. A comparison of modeled versus measured changes is an indication of how well the model will interpret (in terms of diagnosed flux balance) measured temperature changes when they are applied as forcing. The comparison is also an indicator of the performance of the surface and submedium treatments used in this model. Table 2 includes the comparison of the modeled diurnal surface temperature range, compared with that measured by the Visible-Infrared Spin Scan Radiometer (VISSR) instrument on board the GOES geostationary satellite for July 20. The comparison is quite reasonable, with the most noticeable feature being a high relative error in surface temperature range for the wet stations, which, as previously mentioned, developed small cumulus cloud populations.

Figures 3a-3d and 4a-4d each show two examples of model results. Figure 3 shows subjectively the "best" results for the dry and wet experiments, while Figure 4 is a similar display for the "worst" experimental results. In each case, the 12-hour model forecast is shown in comparison to the initial conditions at 1200 UTC and also in comparison to the verification sounding at 0000 UTC.

Accuracy in the predicted height of the mixed layer, while not very important for our purposes, has been extensively evaluated by other MLM investigators as an indicator of model accuracy. In some of the very deep mixed layers which developed in the dry samples, the precise verification height of the mixed layer was very hard to identify (see, for example, Figure 4). Table 2 then also shows the comparison of predicted and verification mixed layer heights subject to errors in manual interpretation of this height from the radiosonde reports.

It is interesting that moisture does not appear to be well mixed in the 0000 UTC verification radiosonde soundings of Figure 3 or in most of the other site verifications, which are not shown. As pointed out by Driedonks and Tennekes

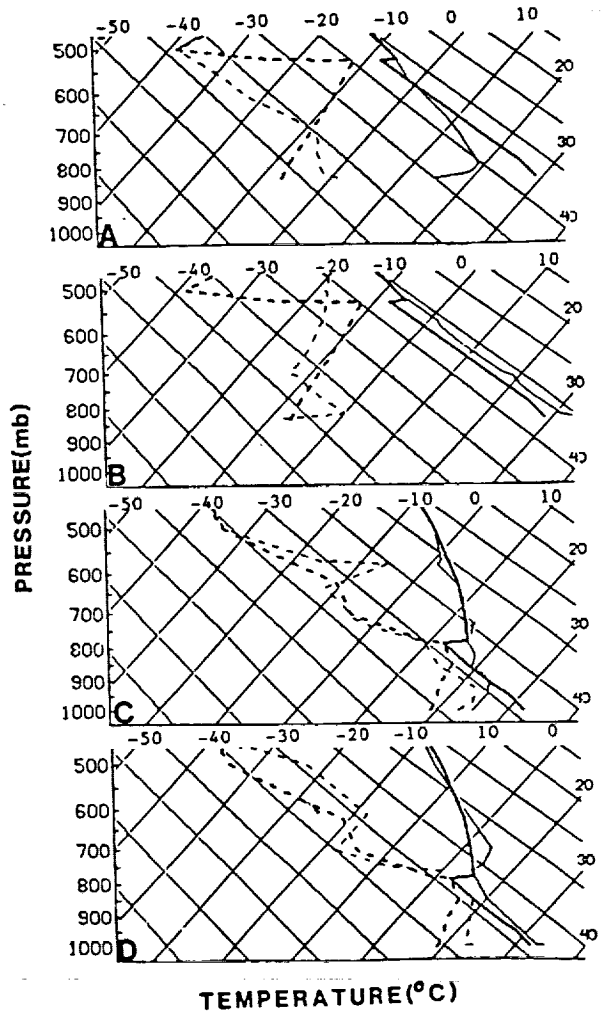

Fig. 4. Same as Figure 2, only for "worst" results. Dry and wet results are stations 576 and 235, respectively.

[1984], it is often observed that moisture frequently exhibits distinct gradients in the daytime PBL and is less successfully treated in MLMs than is potential temperature. Error in the predicted humidity only very weakly influences the structure of other model variables, however, through effects on the vertical gradient of virtual potential temperature used to assess surface layer stability and on the virtual buoyancy flux at H, which influences the growth of the mixed layer.

Initial conditions in the height of the mixed layer and mixed layer mean quantities quickly lose their influence as the mixed layer grows, as pointed out in a mathematical analysis by Driedonks [1982b]. Much of this is due to the fact that the mixed layer height at sunrise is generally quite low compared to the height it reaches at midday under conditions of surfacing heating. Thus the original mass of the PBL, as described by the initial conditions, usually only represents a fraction of the final PBL, and as a result, it has a small influence on the final PBL state, the rest of the influence coming about from fluxes at the surface and the properties of entrainment air. Examining surface flux versus entrainment terms in the MLM for these eight model tests, we found that even for the wet sites (low sensible heating), the change in mixed layer potential temperature due to surface heating was always larger than the warming due to entrainment, by a minimum factor of about 2. For momentum we found that in the dry experiments the mixed layer momentum balance was more influenced by the entrainment process (entrainment flux/surface flux ~2-5) due to rapid boundary layer growth and increasing winds with height. In the wet cases, momentum changes from surface drag and entrainment processes were more nearly equal. In all cases the magnitude of the geostrophic terms were not significant compared with the other two processes.

4. Error Analysis

4.1. Method

Of particular relevance to this work are the effects of errors in measurement of the surface temperature and in the assignment of surface parameters and model boundary conditions on the prediction of surface fluxes, when the model is run in the remote-sensing mode. These systematic and random errors interact in complex ways, which can be best understood on a situation-by-situation basis. Nevertheless, a great deal of insight can be gained by first examining individually the effects of a given measurement error or other error constituent.

The evaluation of the effects of various errors is done via the methodology of the observing system simulation experiment (OSSE). Control model runs are made in the full prognostic mode and "truth" values of the surface temperature, surface fluxes, and mixed layer variables are generated. Subsequently, the model-generated surface temperature time series are used to force the model energetics (remote-sensing mode) in a second integration from the same initial conditions, only in this case, with constituent errors added. An evaluation of the effect of an error can then be made comparing the two model runs. An initial experiment is to run the model in the remote-sensing mode with no errors introduced to insure that the results are exactly the same as the control and thus that the model is internally consistent. This was done for all eight of our samples.

Our investigations have shown that random errors in measurements and other specified quantities do not cause significant errors in flux calculations, and thus this discussion will be confined to the effects of the systematic errors, which can have much larger effects. Similarly, the effects of errors in the MLM upper boundary condition for mixing ratio (γ_q) are small and will not be described. For simplicity, we will discuss errors which cause a positive error in the diagnosis of surface sensible heat flux. The opposite result (negative sensible heat flux error) is always true when the sign of the error constituent is reversed. While it is not possible to explain every feedback mechanism, those with significant contributions will be detailed. In this energy balance scheme the errors in latent heat flux are always approximately equal to the sensible heat flux errors, but of opposite sign.

4.2. Surface Temperature Measurement Error

The model calculation of sensible heat flux is sensitive to the specified surface temperature change and systematic errors in this quantity. A positive error in this applied temperature increases the predicted sensible heat flux (decreased latent heat flux) by increasing the surface-mixed layer potential temperature gradient. A major feedback mechanism is associated with the erroneous momentum entrainment occurring with the over-predicted sensible heat flux and mixed layer growth. In the usual case of winds increasing with height, the result is an overspeeding of the winds and a reinforcement of the positive error in the surface sensible heat flux.

Ground truth confirmation of satellite-measured surface temperature changes over the large spatial scales involved in this study are totally nonexistent. As discussed, however, by Wetzel et al. [1984], random errors in the data are found to be small compared to the precision with which the data are reported. GOES infrared radiancesare converted to digital counts, limiting the precision to 0.5 K. The spatial averaging of data (8 x 8 pixels) and the multiple time samples used in our methods should increase this precision substantially. Our investigations indicate that neglecting the time change of atmospheric corrections to GOES channel 8 temperatures, as is done in our procedures, will at most cause an error of only a few tenths of a degree in 12 hours in the retrieved surface temperature change. We have thus selected a linear addition in time of a total temperature excursion error of 1.0 K as being representative. The result on our control runs was a standard error in sensible heating of 0.523 MJ m^{-2}, which

was 2.4% of the average 12-hour net shortwave forcing for these cases of 22.1 MJ m^{-2}. Errors are largest for the dry cases, mostly because of the nonlinearity of surface fluxes with surface temperature excursion under these highly unstable conditions.

4.3 Roughness Height Errors

The primary effect of errors in the specification of surface roughness (Z_0) is to modify the exchange coefficients for heat, momentum, and moisture at the surface. An increase of surface roughness from a reference value will in general increase surface sensible heating by augmenting the heat transfer coefficient. Since under neutral conditions the coefficient increases as $(\ln Z/Z_0)^{-2}$, increasing Z_0 at lower base roughness heights by a set amount has a much larger effect than at higher values of roughness.

We have assigned large errors in Z_0, increasing from 3 cm at Z_0=1 cm to 25 cm at Z_0=48 cm, partially because of general uncertainties in its evaluation and also to cover general uncertainties in using a simplified surface parameterization scheme.

The result of positive errors in the specification of Z_0 in our control runs was a standard error of 0.441 MJ m^{-2} in 12-hour sensible heating, which represented 2.0% of the average 12-hour net shortwave flux.

4.4. Upper Boundary Condition Error

Diagnosed vertical gradients in θ, U, and V (γ_θ, γ_u, γ_v) form the upper boundary conditions in temperature and momentum for the MLM, as it grows into its environment. Errors in the specification of these quantities become errors in the MLM mean and jump quantities, as air is entrained during the mixed layer rise. These errors can either be interpreted as errors in evaluating the initial conditions, or as time changes in the large-scale environment that occur during the course of the model integration and that are not accounted for.

Approximate error magnitudes for upper boundary conditions in momentum and potential temperature were estimated from the radiosonde data by calculating the 12-hour differences (1200-0000 UTC) of their vertical gradients in the 100 mbar at above the final (0000 UTC) PBL height. The resulting 12-hour standard errors were 1.6 x $10^{-3} s^{-1}$ in the velocity vertical gradient and 1.4 x 10^{-5} °C cm^{-1} for the potential temperature gradient. In subsequent MLM error simulations the errors were added linearly in time between 1200 and 0000 UTC.

Potential temperature boundary condition error. If there is a negative error in the assignment of the vertical gradient of potential temperature γ_θ, air with an erroneously low value of potential temperature is entrained into the mixed layer as it grows, resulting in enhanced mixed layer deepening, increased surface-MLM θ gradient, and increased surface sensible heating. In this case, the error reinforces itself, since the increased surface sensible heat flux further augments the mixed layer growth. Fortunately, even under relatively weak sensible heating conditions, the change in mixed layer θ is most strongly influenced by surface heating. Control runs incorporating a negative potential temperature gradient error of the magnitude discussed in section 4.3 had only small sensible heating errors, less than 1% of the net shortwave flux for 12 hours.

Momentum boundary condition error. A positive error in the vertical gradient of wind, with winds increasing in height, increases surface sensible heating by accelerating model wind speeds as the mixed layer grows and entrains. A major compensation mechanism may exist in the surface momentum drag, which also increases as winds accelerate. Unlike mixed layer potential temperature change, where surface heating usually dominates, the change of mixed layer momentum (evaluated from our model runs) is more nearly a balance between surface drag and entrainment.

The character of the sensible heat flux errors induced by errors in vertical wind gradients are situation-dependent, owing chiefly to the high variability of both mixed layer growth rates (varying importance of entrainment terms in the momentum balance) and the gradient of momentum in the vertical.

A positive error in momentum gradients for our control runs of the magnitude mentioned previously produced only minor sensible heating errors, in all cases less than 1% of the net shortwave flux for 12 hours. Highest errors were for the dry cases with large mixed layer growth and thus higher entrainment of erroneous momentum information.

4.5. Maximum Error

Errors in sensible and latent heating for a given case depend on the nature of the particular situation and the measurement and modeling errors discussed in previous sections, whose directions and magnitudes are generally unknown. Chiefly because of these uncertainties, we have chosen to investigate a "maximum" error, that is, to try and define an upper limit of error expected when individual error components all contribute in the same direction to the evaluation of sensible heat flux (and latent heat flux through energy balance considerations).

The magnitude of the assigned errors in surface temperature change, surface roughness, and wind and potential temperature vertical gradients rates are those discussed in section 4.4. Directions have all been chosen to provide positive errors in the modeled sensible heating, that is, positive errors in surface temperature, vertical wind gradient, and roughness height, and a negative error in potential temperature vertical gradient. In this energy balance scheme, errors in diagnosed latent heat are approximately equal to the sensible heat error, but of opposite sign.

Error runs were produced for the eight wet and dry sites. To increase the sample size, the surface Bowen ratio was varied in five intervals between high evaporation (B_0=0.4) and negligible evaporation (B_0=1000). Roughness heights were similarly varied in five intervals between 1 and

TABLE 3. Errors in Model-Predicated 12-hour Sensible Heating Resulting From Errors in Surface Temperature Measurement, Roughness Height Assignment, and Upper Boundary Conditions for Varying Evaporations and Roughness Regimes

	Z_0, cm											
	1		5.7		11.6		20.1		31.9		48.1	
Bowen Ratio	εQ_0, MJ m^{-2}	$\varepsilon Q_0/SW_n$	εQ_0, MJ m^{-2}	$\varepsilon Q_0/SW_n$	εQ_0, MJ m^{-2}	$\varepsilon Q_0/SW_n$	εQ_0, MJ m^{-2}	$\varepsilon Q_0/SW_n$	εQ_0, MJ m^{-2}	$\varepsilon Q_0/SW_n$	εQ_0, MJ m^{-2}	$\varepsilon Q_0/SW_n$
0.3	1.87	0.08	1.31	0.06	1.31	0.06	0.92	0.04	0.73	0.03	0.72	0.03
0.4	1.84	0.08	1.43	0.06	1.38	0.06	1.32	0.06	1.25	0.05	0.93	0.04
0.5	2.30	0.10	1.94	0.08	1.70	0.07	1.15	0.05	1.13	0.05	1.01	0.04
1.0	3.47	0.15	2.60	0.11	2.07	0.09	1.91	0.08	1.70	0.07	1.20	0.05
2.0	4.40	0.19	3.23	0.14	2.77	0.12	2.73	0.12	2.31	0.10	1.62	0.08
3.0	5.01	0.22	3.72	0.16	3.24	0.14	3.21	0.14	2.60	0.11	2.07	0.09
10.0	6.43	0.28	3.91	0.17	3.69	0.16	3.66	0.16	3.00	0.13	2.51	0.11
1000	6.68	0.29	4.15	0.18	3.91	0.17	3.89	0.17	3.24	0.14	2.77	0.12

Here εQ_0 is the standard sensible heating error, while $\varepsilon Q_0/SW_n$ is the same error normalized to a 12-hour net shortwave flux total of 22 MJ m^{-2}.

TABLE 4. Error in Satellite Experiments (Model Versus Radiosonde) for Model-Predicated Mixed Layer Quantities

STN	$\lvert\overline{\Delta T}\rvert$, °K	$\lvert\overline{\Delta H}\rvert$, mbar	Q_{0c}, MJ m^{-2}	Q_{0s}, MJ m^{-2}	T_{sm}, °K	E_{0c}, MJ m^{-2}	E_{0s}, MJ m^{-2}	B_0	$\Delta E_0/SW_n$
365	1.2	40	13.92	15.54	31.0	0	0	∞	0.074
486	0.9	20	13.99	18.84	30.5	0	0	∞	0.205
476	2.0	10	14.64	15.78	28.5	0	0.12	130	...
576	2.3	70	14.10	15.54	28.0	0	0	∞	0.062
247	2.4	10	5.02	2.80	7.0	13.65	15.80	0.18	...
260	1.6	15	...	8.10	14.5	...	9.93	0.81	...
261	2.3	40	...	9.78	13.0	...	7.52	1.30	...
363	0.31	50	...	10.56	21.0	...	6.23	1.70	...
562	0.48	40	...	13.70	17.5	...	1.97	6.95	...
$\overline{E}$ TOT	1.50	32							

Notation is the same as in Table 2, except that Q_{0c} and Q_{0s} are 12 hour sensible heating totals for control and satellite experiments, respectively; E_{0c} and E_{0s} are similar latent heating totals; B_0 is the calculated Bowen ratio from the satellite experiments; and $\Delta E_0/SW_n$ is the amount by which sensible plus submedium fluxes exceeded the net radiation in the satellite experiments, normalized to the net shortwave flux.

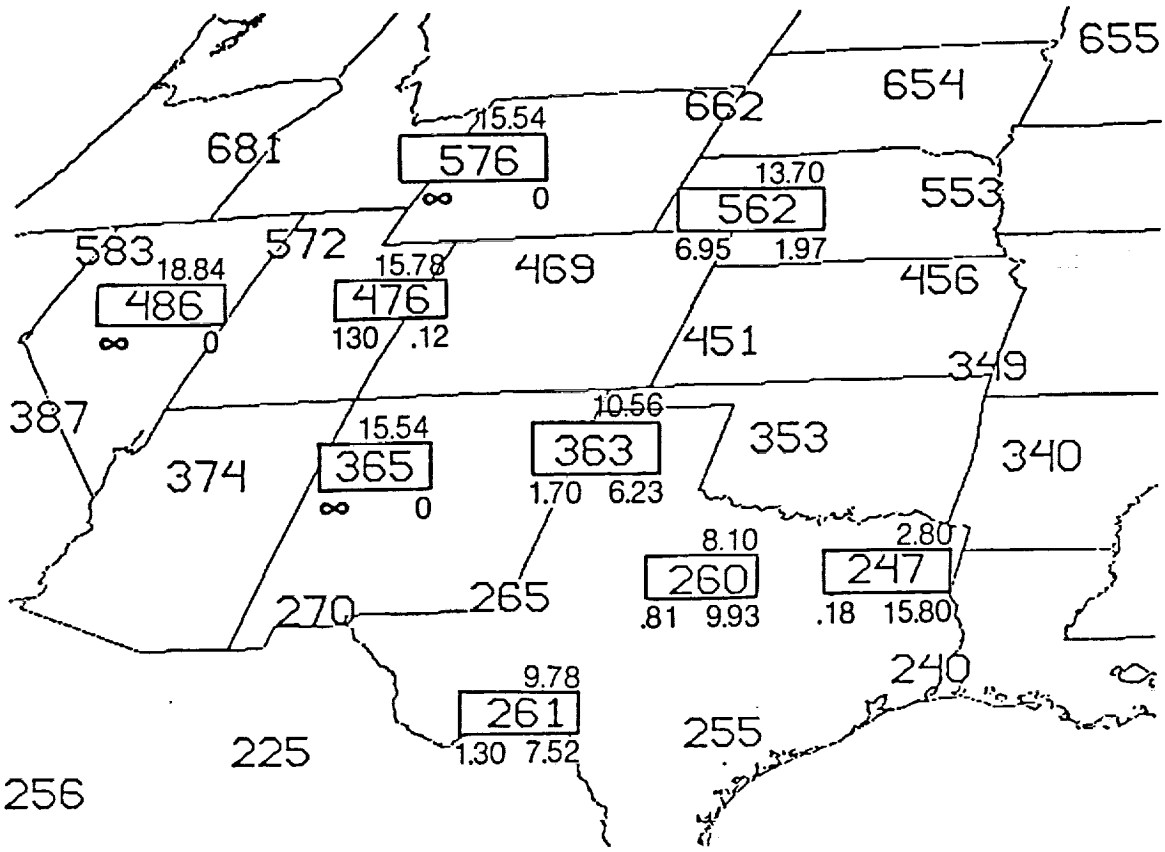

Fig. 5. Spatial variability of 12-hour sensible and latent heating totals from satellite experiments. Boxed numbers indicate radiosonde locations used in the satellite experiments. The number above the box is the 12-hour sensible heating total, while the number below, on the right, is the latent heating for the same period (both MJ m^{-2}). The number below, on the left, is the diagnosed Bowen ratio for the site, calculated from model flux outputs.

48 cm in equal increments of $[\ln(Z_0)]^{-2}$. Thus a total of 200 (8 x 5 x 5) error simulations resulted for various evaporation and roughness characteristics.

A summary of results is shown in Table 3. Shown are the standard energy errors for sensible heat evaluation over different conditions of evaporation and surface roughness character and these errors normalized to the 12-hour net shortwave flux total for the experiments.

It is clear that the total errors are greater than the sum of the individual error components investigated in the previous section, indicating nonlinear interactions between the error constituents. The standard error in sensible heating normalized to 12-hour net shortwave flux in these 200 trials was 0.026, 0.014 and 0.006 for the individual components of T_s, Z_0, and $\gamma_{u,v,\theta}$, respectively. The same standard error for all these error constituents in combination was 0.102. Errors increase with increased sensible heating and decreasing roughness height. The "dry and smooth" regime is most vulnerable to measurement and boundary condition errors. Here small errors in roughness height assignment make the largest differences in transfer coefficients ($[\ln Z/Z_0]^{-2}$) and the model interpretation of surface temperature change in terms of sensible heating. Errors in the surface sensible flux result in significant error in mixed layer growth rates under these high growth conditions and in further positive feedback to the error due to erroneous entrainment of air above the mixed layer. Our investigation indicates that most of the total error is a result of the interaction between surface temperature and roughness height errors, with the contribution from upper boundary condition error adding only a few percent to the error total.

5. Satellite Experiments

5.1. Site Selection

As previously described, small cumulus cloud contamination precluded the use of three out of four of the wet sites in the satellite data experiments owing to resulting errors in the retrieval of surface temperatures. Other station locations were substituted in the central United States across the transition zone of moisture regimes to examine the sensitivity of our methods to evaporation climatology.

It was necessary to violate some of the criteria of ideal observing conditions to have an adequate sample size. Finding cloud-free sites with negligible temperature advection and relatively unchanging large-scale boundary conditions was not possible and points to some of the draw-

backs of the methods which will be discussed in section 6.

The sites for the satellite evaluations are listed in Table 1, along with relevant characteristics.

5.2. Data and Model Logistics

One-hour time changes of surface temperature were constructed from GOES-4 hourly band 8 (11 lm) window channel measurements for July 20, using 8 x 8 pixel boxes (~32 x 32 km) centered on the stations of interest between the hours of 1100 and 0000 UTC. For these experiments the model was initialized at local sunrise time in a prognostic mode with a "guess" surface Bowen ratio (unity) and the 1200 UTC station synoptic sounding. The range of sunrise times for the stations investigated was no more than ±0.5 hour from the synoptic time. At the time when the predicted net radiation trace crossed zero (toward a positive value, positive flux toward the surface), generally about 0.5 hour after sunrise, the surface and submedium temperatures were reinitialized at values producing zero sensible and submedium fluxes. From this point in time, the satellite-measured surface temperature changes were used to force the model out to the 0000 UTC verification hour. Since the model has a time step interval of 10 min, but the GOES measurements are at a coarser time resolution of 1 hour, it was necessary to construct 10-min surface temperature changes for the model by linear interpolation in time between the hourly measurement values.

5.3. Results

The locations used in the satellite evaluation are shown in Figure 5, along with the diagnosed 12-hour sensible heating results from the model. The number above the station (shown in boxes) is the 12-hour sensible heating in megajoules per square meter, and the number below, on the right, is the latent heating total. The number below, on the left, of the station is the Bowen ratio, calculated for the site from model flux outputs. The numbers appear quite spatially coherent and depict well the sharp change in surface moisture climatology across the central United States, although the limitations indicated by the error analysis of the previous section must be kept in mind.

Comparison with 0000 UTC radiosonde verification for these MLM simulations is shown in Table 4, and a selection of model-generated soundings going across evaporation regimes is shown in Figure 6. The results are encouraging, in that they are close to those obtained from the benchmark model experiments of section 3.

An independent error check for sites in arid areas is whether the diagnosed sensible heat flux plus submedium heat flux exceeds the estimated net radiation. In this instance, through energy balance considerations, there would be a latent heat flux toward the surface, a physically unrealistic condition. This has happened at three sites, as shown in Table 4, and here the latent heat flux has been readjusted to zero.

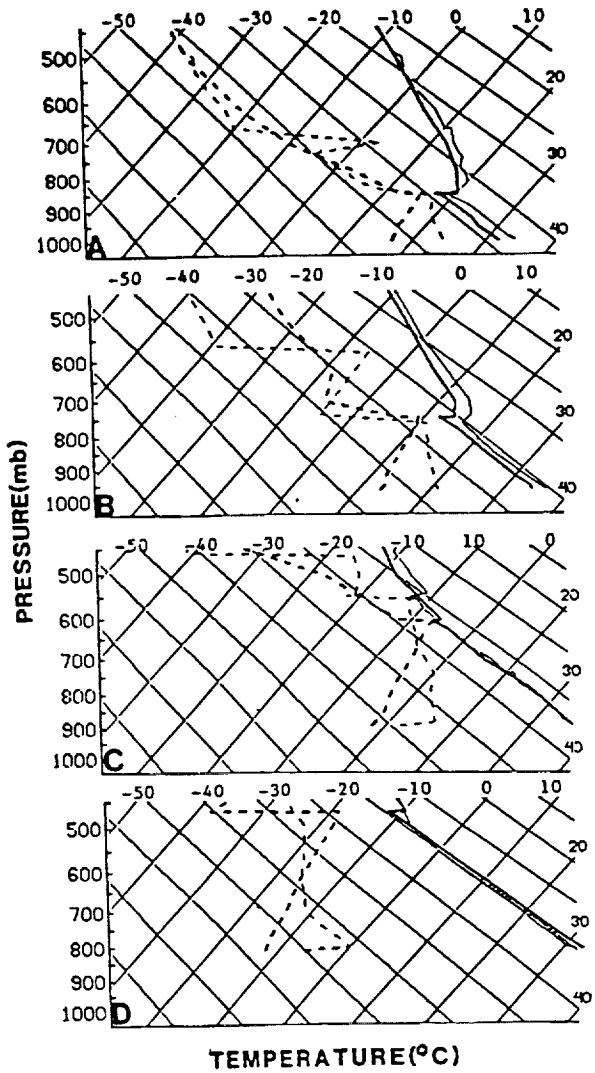

Fig. 6. Skew T - log p diagram of temperature and dew-point temperature (in degrees Celsius) versus pressure (in mbar) for satellite data MLM runs across transition region of evaporation regimes. Station sequence is 247, 260, 363, and 486 for Figures 6a, 6b, 6c, and 6d, respectively. The dark and light lines are model prediction and radiosonde verification, respectively.

The amount by which $Q_0 + G_0$ exceeded the net radiation at these sites (e.g., the approximate error in latent heat flux) is also shown in Table 4, normalized to the net shortwave flux. As can be seen, the errors are well within the approximate error bounds of the methods established in section 4 and Table 3.

The most obvious error in these satellite experiments is a low bias in the predicted mixed layer temperatures for stations 247 and 260 (Figures 6a and 6b). As Figures 6a and 6b show, atmospheric temperatures have changed noticeably above the height of the PBL, suggesting strongly that the nonadvection requirement has been violated. The nature of the Texas region where these two stations are located suggests a potential reason why our evaluation of advection from a limited area model could have been in error. During the 12-hour period investigated,

TABLE 5. Brightness Temperature Changes for VAS Channels 5-8 Versus 12-hour Sensible Heating Totals for Various MLM Experiments

Q_0, MJ m^{-2}	VAS Channel Brightness Temperature, °K			
	5	6	7	8
4.2	274.95	270.01	289.11	292.83
5.1	275.00	270.03	289.21	292.89
5.9	275.04	270.06	289.33	292.93
10.9	275.23	270.37	289.72	292.95
12.5	275.63	270.68	289.72	293.11
15.6	275.68	270.72	289.78	293.13

the low level winds at these stations were from the SSE to SSW. This fact, along with the proximity of the Gulf of Mexico, a large synoptic data void, suggests that the model-evaluated advection might have been in error owing to errors in the initial conditions in the limited area model.

Of interest for stations 247 and 260 is that while mixed layer temperatures are underpredicted by the MLM using measured surface temperatures as forcing, the height of the mixed layer is predicted quite well. The growth of the mixed layer under nonadvective conditions and surface solar forcing is almost always dominated by the amount of surface sensible heating. Although it will need to be verified in subsequent observational and modeling studies, it can be hypothesized that the growth of the mixed layer would be more influenced by vertical differential advection (above and below the mixed layer height) than by advection through a deeper layer. If this is true, then the accuracy of the predicted mixed layer heights for stations 247 and 260 would indicate that the surface energy balance evaluation at these sites is not greatly influenced by the deep advection processes, which the synoptic soundings indicate are taking place.

6. Conclusions and Future Research

A method has been presented to evaluate sensible heat flux and latent heat flux through energy balance, using geostationary satellite-measured surface temperatures in a mixed layer model representation of the atmospheric boundary layer. The methods have been applied to assess the regional variation of fluxes across the sharp transition zone of evaporation climatology in the central United States. While errors in the evaluation are highly situation-dependent, an error analysis indicates that maximum daily sensible heat flux errors would be of the order of 10% of net solar radiation for wet regimes and about double this for very dry situations, making perhaps five divisions of evaporation conditions identifiable. While these results are from a surface model which is very simplified, the main cause of error is the interaction of surface temperature error with errors in surface transfer properties (Z_0), errors which have counterparts even in more sophisticated models. The primary accuracy limitation thus stems from the ability to measure and characterize the surface, rather than from model sophistication. Further work will need to address the topics of the spatial variability of surface temperature and atmospheric data and appropriate matching of scales and also the effects of local variabilities in large-scale processes (advection, etc.) on the flux diagnoses.

A strong point of the MLM remote-sensing technique explored in this paper is the low dependence of the results on the exact atmospheric initial conditions. This implies that three-dimensional analyses of the atmosphere, similar to those currently used to initialize regional numerical prediction models, could be substituted for the radiosonde reports used in this study to initialize the MLM. Thus evaluation of surface fluxes could be done away from radiosonde locations and subsynoptic features quantified.

Some of the sampling constraints (no advection, no clouds, no mesoscale circulations), however, are formidable and will dictate inherent limitations on how often an area may be evaluated and thus also on the time scale of the features which will be resolvable. These problems have certain parallels with the developing concepts of four-dimensional data assimilation (4DDA) in dynamic meteorology, which is currently a topic of intense investigation in the research community. The object of 4DDA is to produce the best possible four-dimensional description of the atmosphere given data sources which have widely varying spatial and temporal sampling characteristics as well as varying accuracies. A forecast model is invariably used to integrate the effects of measurements over space and time.

A similar system can be envisioned for land surface processes, where the remote-sensing system and an analysis/forecast model are used in a complementary manner. The remote-sensing procedures would be used to "update" the surface energy budget parameters used in the forecast model whenever possible, while the analysis/forecast model would, in turn, be used as a tool to evaluate when conditions are appropriate for remote sensing and to compensate when possible for processes such as advection (to relax sampling limitations). Such a system ideally should be flexible enough to incorporate new types of measurements of the surface energy balance as they are developed. New satellite instruments proposed to fly in the next 10 years may relax the dependence on surface temperature and make alternative techniques possible. To conclude this discussion, we will briefly mention several interesting possibilities.

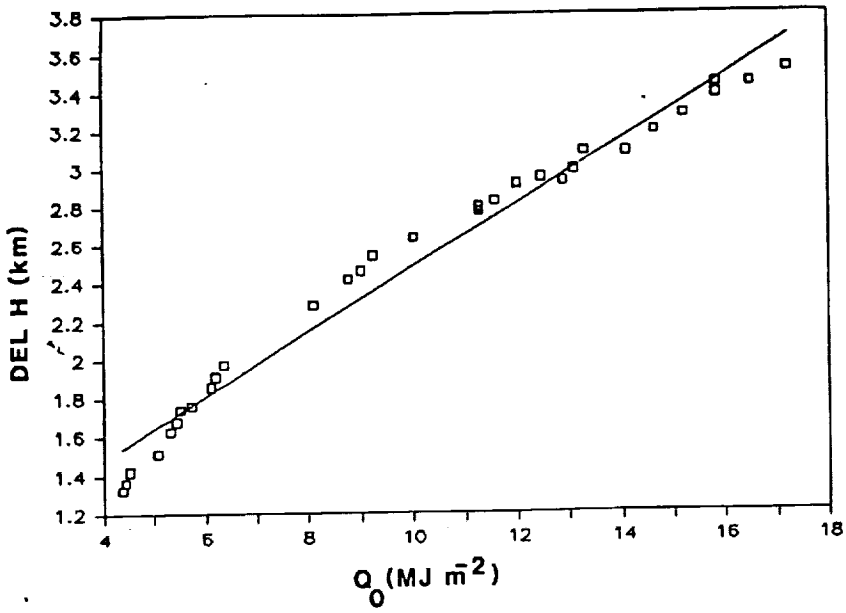

Fig. 7. Twelve-hour change in height of mixed layer versus 12-hour sensible heating total for MLM runs.

Table 5 shows simulated brightness temperature (from a forward radiance model and 12-hour MLM forecast temperature changes) for several channels of the VISSR Atmospheric Sounder (VAS) instrument on board the current series of geostationary satellites. The channels shown receive atmospheric thermal radiation from sequentially lower regions of the atmosphere with increasing channel number. All the channels shown may detect radiation both from the lower atmosphere and surface. In Table 5 the surface temperature contribution to brightness tempera-ture has been removed through knowledge of the surface temperature from the MLM. The changes in brightness temperature between MLM runs varying the surface sensible heating then are entirely from changes in atmospheric temperatures induced by this sensible heating. The signal is quasi-independent of surface type.

Unfortunately, the idealized signals shown in Table 5 are only very marginally separable using the VAS instrument. First, the channels shown in Table 5 have an instrument noise level of about 0.3 K. Second, in practice, it is only realistically possible to make the required correction for the surface temperature change in the total brightness temperature change to an accuracy of a few tenths of a degree. Sounders proposed for the 1990's [see Smith et al., 1979], which will make radiance measurements at a much finer spectral resolution (several thousand channels in the 3- to 14-μm region, as opposed to 12 channels for the VAS), will offer more than a factor of 2 in vertical resolving power over current instruments. This will result in substantially larger atmospheric brightness temperature signatures of the type shown in Table 5 as a result of resolution of the PBL. Also, the surface contribution will be more accurately removed, using the very clean window channel information which will be obtainable with the new instrumentation.

Our limited experience, to date, in trying to use lower atmospheric radiance signatures to diagnose surface fluxes indicate that their exact character will vary somewhat, depending on the initial state of the atmosphere before onset of PBL growth. Our initial investigations in quantifying these signals will proceed along the same general lines as the so-called "physical" retrieval method, used to retrieve atmospheric profiles of temperature and moisture from satellite radiance measurements (see, for example, Smith [1983]). In these methods a "guess" profile of the atmosphere (usually a numerical prediction) is used to calculate first guess atmospheric radiances. The difference between satellite-measured and guess radiances is subsequently the "signal," which is used to improve the guess atmospheric profile of temperature and moisture. We plan to investigate a similar technique for evaluation of surface fluxes using the MLM prediction (with initial guess values of surface moisture parameters) to establish the first guess atmosphere and radiances and subsequently to quantify how deviations in measured minus guess radiances relate to differences in surface fluxes for varying atmospheric situations.

The strong dependence of the height excursion of the PBL on surface fluxes is another signal which potentially can be exploited to yield information on land-surface processes. Figure 7 shows the 12-hour change in mixed layer heights (DELH) predicted in MLM simulations, with a variety of Bowen ratios and roughness values, as a function of the 12-hour sensible heating totals from the same model runs. The initial conditions used in the set of model simulations that are displayed in Figure 7 were from synoptic station 247. Initializing the MLM with radiosonde soundings from the other model test sites described in section 3, representing a large range of initial conditions in temperature

moisture and wind speeds, yielded results similar to those shown in Figure 7. Of importance is the finding that across this large range of surface parameters and atmospheric conditions there is a very strong relationship between mixed layer growth and sensible heating. The basic linear fit of DELH to S_0, shown in Figure 7, has only about a 100-m standard error in DELH, implying that from a measurement of DELH that sensible heating could be deduced to an accuracy of about 1 MJ m^{-2}, even when knowledge of atmospheric conditions is basic. This accuracy is several times better than the statistics in Table 3 suggest is attainable using surface temperature measurements, even when atmospheric conditions are well understood. Similar observations for the growth of the marine boundary layer in a case study of a cold-air outbreak over the Gulf Stream have been made by Chou and Atlas [1982], who concluded that "the growth of the boundary layer and sensible heating may be used as proxies for one another."

At synoptic sites the general assessment of sensible heat flux from DELH shown in Figure 7 could be refined by using the specific radiosonde sounding to initialize the MLM and by varying the surface sensible heating in a series of simulations around a "guess" value (the previous day's results or climatology, for example), until the prediction of PBL height excursion matches the observed value.

While indications are that techniques using the PBL height to diagnose fluxes will be more accurate than schemes using surface temperature measurements, for the present their use will be limited to synoptic locations where DELH can be evaluated. As previously discussed, surface temperature measurements have some potential for subsynoptic scale evaluation of surface fluxes. Two possibilities which we will be exploring in future research are the use of the DELH method to "calibrate" surface temperature methods at synoptic locations and the use of surface temperature measurements to fill in the horizontal gradients of sensible and latent heating between radiosonde measurements of their absolute values.

One of the most interesting prospects for the use of PBL height excursion to diagnose surface fluxes will come with the launch of the space-based lidar system planned for the 1990's. The accuracy goal for the proposed Lidar Sounder and Altimeter (LASA) instrument is 50 m in the retrieval of PBL depth [Curran, 1987]. Chou and Atlas [1982] have already suggested the utility of such a space-based measurement for assessment of ocean-surface fluxes during cold-air outbreaks. The fact that the growth of the land-surface PBL depends highly on surface sensible heating and less importantly on specific atmospheric conditions suggests that this lidar system will also be very beneficial in monitoring land-surface energetics between synoptic locations and in the many areas of the globe where atmospheric information is sparse.

Acknowledgments. This work was supported under the NASA Interdisciplinary Satellite Land Surface Climatology Program (ISLSCP), grant NAG5-854. Thanks go to fellow CIMSS and NESDIS scientists for their consultations and to Laura Beckett for skillfully preparing the manuscript.

References

Benjamin, S. G., and T. W. Carlson, Some effects of surface heating and topography on the regional severe storm environment, Mon. Weather Rev., 114, 307-329, 1986.

Boers, R., F. W. Eloranta, and R. L. Coulter, Lidar observations of mixed layer dynamics: Tests of parameterized entrainment models of mixed layer growth rates, J. Clim. Appl. Meteorol., 23, 248-266, 1984.

Bryson, R. A., and F. K. Hare (Eds.), Climates of North America, World Surv. of Climatol., vol. 11, 420 pp., Elsevier-Scientific, New York, 1974.

Buettner, K., and D. Kern, The determination of infrared emissivities of terrestrial surfaces, J. Geophys. Res., 70, 1329-1337, 1965.

Businger, J. A., J. C. Wyngaard, Y. Izumi, and F. F. Bradley, Flux profile relationships in the atmospheric surface layer, J. Atmos. Sci., 24, 181-189, 1971.

Carlson, T. N., J. K. Dodd, S. G. Benjamin, and J. N. Cooper, Remote estimation of the surface energy balance, moisture availability and thermal inertia, J. Appl. Meteorol., 20, 67-87, 1981.

Chou, S., and D. Atlas, Satellite estimates of ocean-air heat fluxes during cold air outbreaks, Mon. Weather Rev., 110, 1434-1450, 1982.

Curran, R. J. (Ed.), LASA, Lidar Atmospheric Sounder and Altimeter, Earth Observ. Syst. Rep. IId, 91 pp., NASA, 1987.

Deardorff, J. W., Parameterization of the planetary boundary layer for use in general circulation models, Mon. Weather Rev., 100, 93-106, 1972.

Diak, G. R., and C. Gautier, Improvements to a simple physical model for estimating insolation from GOES data, J. Appl. Meteorol., 22, 505-508, 1983.

Diak, G. R., S. Heikkinen, and J. Bates, The influence of variations in surface treatment on 24-hour forecasts with a limited area model, including a comparison of modelled and satellite measured surface temperatures, Mon. Weather Rev., 114, 215-232, 1986.

Driedonks, A. G. M., Models and observations of the growth of the atmospheric boundary layer, Boundary Layer Meteorol., 23, 284-306, 1982a.

Driedonks, A. G. M., Sensitivity analysis of the equations for a convective mixed layer, Boundary Layer Meteorol., 22, 475-480, 1982b.

Driedonks, A. G. M. and H. Tennekes, Entrainment effects in the well-mixed atmospheric boundary layer, Boundary Layer Meteorol., 30, 75-105, 1984.

Fuchs, M., and C. B. Tanner, Infrared thermometry of vegetation, Agron. J., 58, 239-253, 1966.

Hummel, J. R., and R. A. Reck, A global surface albedo model, J. Appl. Meteorol., 18, 239-253, 1979.

Kanemasu, E. T., L. R. Stone, and W. L. Powers, Evapotranspiration model tested for soybean and sorgum, Agron. J., 68, 569-572, 1976.

Kasahara, A., and W. Washington, General circulation experiments with a six-layer NCAR model, including orography, cloudiness, and surface temperature calculations, J. Atmos. Sci., 28, 657-701, 1971.

Kondrat'yev, K. P. A., Radiation in the Atmosphere, 859 pp., Academic, San Diego, Calif., 1969.

Kung, E. C., R. A. Bryson, and D. H. Lenschow, Study of a continental surface albedo on the basis of flight measurements and structure of the Earth's surface cover over North America, Mon. Weather Rev., 92, 543-564, 1964.

Lettau, H. H., and K. Lettau, Exploring the world's driest climate, IES Rep. 101, 264 pp., Cent. for Clim. Res., Inst. for Environ. Stud., Univ. of Wisc. Madison, 1978.

Matthews, E., Prescription of land-surface boundary conditions in GISS GCM 11: A simple method based on high-resolution vegetation data bases, NASA Tech. Memo 86096, 20 pp., Goddard Space Flight Center, New York, 1984.
boundary layer model, J. Appl. Meteorol., 14, 289-296, 1975.

Oke, T. R., Boundary Layer Climates, 372 pp., John Wiley, New York, 1978.

Peterson, R. A., D. Keyser, A. Mostek, and L. Uccellini, Severe storms analysis and forecasting techniques using VAS satellite data. Proc. 13th Conf. Severe Local Storms, Boston, AMS, 375 pp., 1983.

Price, J., On the use of satellite data to infer fluxes at meteorological scales. J. Appl. Meteorol., 21, 1111-1112, 1982.

Schmugge, T. J., T. J. Jackson, and H. L. McKim, Survey of methods for soil moisture determination, Water Resour. Res., 16, 961-979, 1980.

Sellers, W. D., Physical Climatology, 272 pp., University of Chicago Press, Chicago, Ill., 1965.

Sellers, P. J., Y. Mintz, Y. C. Sud, and A. Dalcher, A simple biosphere model for use within general circulation models, J. Atmos. Sci., 43, 505-531, 1986.

Smith, W. L., The retrieval of atmospheric profiles from VAS geostationary radiance observations, J. Atmos. Sci., 40, 2025-2035, 1983.

Smith, W. L., P. K. Rao, R. Koffler, and W. R. Curtis, The determination of sea surface temperature from high-resolution infrared window radiation measurements, Mon. Weather Rev., 98, 604-611, 1970.

Smith, W. L., H. B. Howell, and H. M. Woolf, The use of interferometric radiance measurements for sounding the atmosphere, J. Atmos. Sci., 36, 566-575, 1979.

Smith, W. L., V. E. Suomi, F. X. Zhong, and W. P. Menzel, Nowcasting applications of geostationary satellite atmospheric sounding data, in Nowcasting, pp. 123-135, Academic, San Diego, Calif., 1982.

Suarez, M. J., A. Arakawa, and D. Randall, The parameterization of the planetary boundary layer in the UCLA general circulation model: Formulation and results, Mon. Weather Rev., 111, 2224-2243, 1983.

Taconet, O., T. Carlson, R. Bernard, and D. Vidal-Madjar, Evaluation of a surface/vegetation parameterization using satellite measurements of surface temperature, J. Clim. Appl. Meteorol., 25, 1752-1767, 1986.

Taylor, E., Measured emissivity of soils in the southeast United States, Remote Sens. Environ., 8, 359-364, 1979.

Taylor, E., Measured emissivity of soils in the southeast United States, Remote Sens. Environ., 8, 359-364, 1979.

Wetzel, P., D. Atlas, and R. Woodward, Determining soil moisture from geosynchronous satellite infrared data: A feasibility study, J. Clim. Appl. Meteorol., 23, 375-391, 1984.

Yan, H., and R. A. Anthes, The effect of variations in surface moisture on mesoscale circulations, Mon. Weather Rev., 116, 192-208, 1988.

Zilitinkevich, S. S., Comments on "A model for the dynamics of the inversion above a convective boundary layer," J. Atmos. Sci., 32, 991-992, 1975.

G. R. Diak and T. R. Stewart, Cooperative Institute for Meteorological Satellite Studies, 1225 West Dayton Street, Madison, WI 53706.

(Received April 18, 1988;
revised January 19, 1989;
accepted January 23, 1989.)

Evaluation of Heat Flux, Moisture Flux and Aerodynamic Roughness at the Land Surface from Knowledge of the PBL Height and Satellite Derived Skin Temperatures

George R. Diak

Cooperative Institute for Meteorological Satellite Studies

(CIMSS)

1225 West Dayton Street

Madison, Wisconsin 53706

April 25, 1989

ABSTRACT

A simple method is presented to evaluate land surface sensible/latent heating and an effective surface roughness over synoptic scales using synoptic station atmospheric measurements of the height of the planetary boundary layer and geostationary satellite measurements of the diurnal surface skin temperature range. In the method a combination surface layer-mixed layer model is used to relate these two measurement quantities to the land surface energetics at a particular location. A preliminary error evaluation suggests that errors in determining the 12-hour surface sensible/latent heat fluxes will be about 1 $MJ\text{-}m^{-2}$ over a large range of surface climatologies.

1. Introduction

Remote evaluation of the partitioning of the net radiation at the earth's surface into sensible, latent and submedium fluxes has been a topic of investigation in the satellite remote sensing community for more than a decade. Increasing capabilities in this area, as discussed by numerous authors, will be of great benefit in the areas of climate and weather modelling, hydrology, agriculture and many related fields.

Most of the satellite remote sensing methods designed to measure the land surface energy balance (SEB) over regional and larger spatial scales have in one way or another used infrared measurements of surface skin temperature with statistical or physical models of the atmospheric surface layer and/or planetary boundary layer (PBL) to infer the flux balance. A drawback in using these skin temperatures or their diurnal range for this purpose is that the temperature signals are not uniquely dependent on the flux balance, but also depend on the atmospheric state

and, very importantly, the character of the particular land surface. The surface roughness, which is important element of the resistance of the surface to aerodynamic transfers, is an important modulator of the surface temperature for a given surface energy balance and atmospheric condition. Other salient characteristics of the land surface and overlying vegetation (for example the biomass, ratio of bare soil to canopy cover, leaf area index, etc.; see Sellers et al., 1986) influence the surface temperature response to solar forcing in ways which the research community is just beginning to understand and successfully model and predict. For quantitative purposes over large spatial scales the surface roughness is very poorly understood as are the other canopy properties mentioned. While some qualitative insight into their spatial and temporal distributions has been obtained through vegetation and land use surveys and satellite data studies, the effects of using these determinations for quantitative surface flux remote sensing purposes are highly uncertain and equally poorly understood.

These sorts of uncertainties can be very detrimental when trying to evaluate surface fluxes from measurements of surface skin temperature or its time change. Examples are shown in Table 1, across the potential range of surface sensible heating values, of the flux errors which result from using remotely-measured surface temperatures in a planetary boundary layer (PBL) model to evaluate the surface sensible heating, taking into account typical uncertainties in the determination of surface roughness, surface temperature and atmospheric boundary conditions. More details on this flux error evaluation may be found in Diak and Stewart (1989, henceforth DS). While the model (to be described) is only of medium complexity, it has been demonstrated by DS

and other researchers that models of this sort can adequately predict the surface temperature response to solar forcing and atmospheric and soil boundary conditions when the surface moisture and surface roughness are correctly specified. As this table shows, especially in the high sensible heating and low surface roughness regime, these flux errors can be a significant fraction of the net solar radiation. The reason for the high errors in this regime is easily understood. Surface layer theory predicts that aerodynamic transfer resistance is proportional to approximately $(\ln(Z/Z_0))^2$, where Z is the height above the surface and Z_0 is the surface roughness. The larger relative uncertainties in this roughness at low values make large differences in the evaluation of the transfer resistance and make correspondingly large differences in a remote evaluation of sensible heating from skin temperature measurements. If latent heating is also evaluated through energy balance considerations in the remote sensing method, errors in this evapotranspiration term will be approximately the same magnitude as the sensible heating error, but of opposite sign.

As investigated in theory by Driedonks (1982a), for the marine boundary layer by Chou and Atlas (1982) and in our own recent investigations (DS), the diurnal rise of the height of the PBL during conditions of surface forcing is highly dependent on the time integral of the surface sensible heat flux. In this study we present a simple method to use this signal, the daytime rise of the PBL height, combined with coincident satellite skin temperature measurements to evaluate sensible heating and the effective surface roughness for heat transfer at synoptic locations.

In this method, multiple runs of a combination surface layer-mixed layer model are made, varying the values of surface moisture and roughness length around climatological means, and initializing the model with a set of atmospheric conditions from the synoptic report. The appropriate values of the surface moisture variable and roughness length for the site are then selected from this ensemble as the ones which when used in the model have simultaneously produced the measurement values of the PBL height rise and surface skin temperature range. The measurement of the PBL height rise comes from the synoptic station data, while the measurement of the skin temperature range is from geostationary satellite information.

2. Surface Layer-Mixed Layer Model (MLM)

The MLM used in this investigation has been thoroughly described in DS and will only be summarized here. The model is a coupled surface layer-mixed layer formulation and is displayed schematically in Figure 1 (A list of symbols is given in Appendix A.) In the surface layer, Monin-Obukov scaling relationships are used to describe the profiles of wind speed, moisture and temperature and the surface layer turbulent fluxes. A surface energy balance equation and submedium formalism shown in this figure are used to calculate the surface temperature response and submedium fluxes. Currently a Bowen ratio (B_0=ratio of sensible to latent heat) and surface roughness (Z_0) are used to parameterize the surface moisture and aerodynamic transfer characteristic, respectively.

Above the surface layer, a mixed layer formulation describes the time change of the atmospheric PBL. The characteristics of mixed layer models have been discussed by many authors. The reader is referred to

excellent discussions by Driedonks and Tennekes (1984) and Driedonks (1982b) for more details. The observed structure of the mixed layer leads to these so-called slab or jump models, where the vertical distribution of potential temperature, momentum and mixing ratio are taken as independent of height and at the top a "jump" in these variables indicates a transition to the stable air above. Closure of the mean quantity and jump equations shown in Figure 1 requires a formalism to specify dH/dt, the change of the mixed layer height in time. The closure assumption shown in the dH/dt equality in Figure 1 is from Zilitinkevich (1975) and is derived from the turbulent kinetic energy budget equation at the mixed layer height. This particular form includes terms for entrainment at the top of the mixed layer and mixed layer storage. Descriptively then, MLM's predict through conservation relations the evolution of layer mean quantities, jumps at the top of the mixed layer and the mixed layer height. Mean quantities change value through the difference between the fluxes at the mixed layer base (input from the surface layer) and corresponding fluxes at H, which are realized through mixed layer growth and resulting entrainment processes. The growth of the mixed layer is fueled primarily by the production of buoyant kinetic energy generated by surface heating and also by mechanical turbulence generated by the surface momentum flux. The time change of jump quantities reflects the balance between surface fluxes and the entrainment and the vertical gradients in the free atmosphere above Z=H.

Our previous investigations (DS) and those by other researchers have shown the mixed layer models to be very accurate in describing the height and structure of the PBL under conditions when surface forcing

dominates the time change of the PBL structure (low values of horizontal advections, no intense mesoscale circulations). With measured surface fluxes as input to the mixed layer model, the height rise and air temperature of the PBL were predicted with RMS accuracies of a few tens of meters and several tenths of a degree C, respectively, in a study by Driendonks (1982b). In DS we found that even using parameterized surface fluxes derived from climatological surface indices (albedo, B_0, Z_0) acting in the surface layer model, that the mixed layer height rise and temperature were predicted to accuracies of 22 mb and 1.7 degrees C, respectively. For remote sensing purposes the mixed layer model formalism has the additional benefits that it is computationally inexpensive and it conserves heat, moisture and momentum.

3. Theory

In DS we investigated the possibility of using surface skin temperatures in the MLM for the remote sensing of surface turbulent fluxes. In that study, the sensitivity of the growth of the mixed layer height to the land surface energy balance became evident. The methodology to be outlined here is simple and relies on now having two measurement quantities, both of which contain information on the surface energy balance and the surface roughness. These measurements are the rise of the mixed layer height (DH) estimated at radiosonde locations and secondly the diurnal range of surface skin temperature (DT_s) as estimated by geostationary satellites.

The dashed lines in Figure 2a show the 12-hour rise in mixed layer height predicted in a series of MLM simulations as a function of surface Bowen ratio and surface roughness. Recall, as outlined in the previous

section, that research tests of MLM's show that they are extremely accurate in the prediction in the time change of mixed layer height when accurate surface fluxes are used as input into the model. The initial atmospheric conditions used in this set of model simulations were from a specific synoptic station in the southeast United States (wet surface moisture conditions, high roughness) at 12 UTC on 20 July 1981. The ranges of B_0 and Z_0 shown in this figure have been selected to bracket the climatological means for this location which were estimated from land use and vegetation information. As demonstrated in this figure, there is a very strong relationship between mixed layer growth and surface heating (surface energy balance). This is due to the fact that under conditions of surface heating the thermally induced buoyancy flux usually is the largest mechanism for PBL growth. Other PBL growth mechanisms are mechanical turbulence (influenced by surface roughness, windspeed and atmospheric stability) and wind shear across the top of the PBL. In this regime of high surface moisture (relatively low sensible heating) the effects of roughness height on mixed layer growth are also easily seen in this figure and are due to the modulations in mechanical turbulence caused by Z_0 variations.

The solid lines in Figure 2a show the predicted diurnal skin temperature range as a function of B_0 and Z_0 from the same series of MLM simulations. As intuitively expected, the highest temperature range is produced at high B_0 and low Z_0 values (large surface sensible heating, higher heat transfer resistance), while lower temperature range values are found in the wetter and rougher regions of the domain.

Figure 2b shows the results of a similar set of MLM simulations as 2a, but for a synoptic location in the western United States which

climatologically has much lower surface moisture and roughness. As shown by the dashed lines in this figure, the dominating influence on the growth of the mixed layer over much of the domain is surface sensible heating (reflected in the B_0 values) and the magnitude of the mixed layer growth is much larger than for the wet regime shown in 2a. The values of the surface skin temperature range are also much larger than in the previous figure. With the large values of surface sensible heating due to high B_0 and high resistence to heat transfer due to low Z_0, the surface temperature rises dramatically. As shown in the figure, there are strong dependencies of the temperature range both on the Bowen ratio and roughness height which vary with location in the figure.

It can be seen in principle then that with the measurements of the quantities DH and DT_s and expressing these two quantities in the following manner

$$DH = F(B_0, Z_0) \qquad (1)$$

$$DT_s = G(B_0, Z_0) \qquad (2)$$

we have two equations in two unknowns and it is possible to solve for both the surface Bowen ratio and the surface roughness height at a location provided that suitable functional relationships for F and G can be determined. As shown in Figures 2a and 2b, we have been able to successfully determine F and G through the use of an ensemble of forecast model predictions which establish the sensitivity of DH and DT_s to B_0 and Z_0 for a specific atmospheric situation. It can be seen in these figures that for any DH, DT_s measurement pair that the solution to

equations 1 and 2 for B_0 and Z_0 is the intersection of the appropriate DH and DT_s isolines for this set of atmospheric conditions.

4. Experiments

The day selected for a case study evaluation of the techniques outlined in the previous section is 20 July 1981. This day has been investigated by DS in a study assessing the utility of satellite-measured surface temperatures in remote sensing of the surface energy balance, by Diak et al. (1986) in a study of the effects of boundary layer processes on limited area forecasts and by several other groups (Smith et al., 1982; Peterson et al., 1983) because of the intense tornado episode which occurred in the Midwest late in the day. Much of the continental United States was cloud free on this day. Areas of cloudiness and precipitation were found in the New England states associated with an eastern Great Lakes low pressure center and also in the upper Midwest and Plains states as a result of a cold front slowly descending through the region during the course of the day.

The day was one of intense contrasts in soil moisture conditions across the continental United States. The antecedent precipitation index (API) is considered to be the best ground truth approximation to area-average soil moisture available on a routine basis over large areas (Wetzel et al., 1984). Our calculation of API for the 30 days preceding July 20 showed extremely dry conditions (API close to 0) westward to the California border from a north-south line extending from central North Dakota through the Texas panhandle. Most areas east of this line had API values closer to the climatological average.

The ten synoptic sites selected on 20 July for this case study evaluation are shown in Figure 3. They have been selected to span the intense climatological transition zone of surface moisture and surface roughness in the central United States. The goal of the experiment was to produce for each of these stations an ensemble of MLM runs, similar to those shown in Figure 2a and 2b, and establish the sensitivity of DH and DT_s to B_0 and Z_0 for each location. Subsequently, the values of B_0 and Z_0 appropriate to the locations are chosen from the ensemble of results. With synoptic data at 12-hour intervals used to establish the mixed layer height rise and the geostationary satellite measuring the diurnal surface temperature range, values of B_0 and Z_0 which simultaneously produce these measurement values in model simulation are selected.

For each ensemble of model runs the MLM was initialized using the 12 UTC synoptic station values of temperature, humidity and windspeed. Because of the nature of the model, which does not yet include advective processes, it was necessary to limit test sites to locations where advection was not large. Temperature advection over 12 hours was evaluated using a limited area model run (Diak et al., 1986) and found to be relatively small at lower atmospheric levels for the selected sites. Each of the locations exhibited a distinct initial (12 UTC) and final (00 UTC) height of the PBL so that it was possible to establish with confidence a 12-hour PBL height rise value from these synoptic reports of temperature, moisture and windspeed.

Since the remote sensing methodology requires that the diurnal temperature range be evaluated from infrared satellite measurements, it was also necessary that the test locations be mostly cloud-free. The

diurnal surface skin temperature range at the locations was constructed from GOES-4 hourly band 8 (11 μm) measurements using 8 x 8 pixel boxes (~32 x 32 km) beginning at 12 UTC. The measurement values of DH and DT_s are shown for each station location in Table 2.

The model surface parameterization (see Figure 1) requires the inputs of surface albedo and emissivity. The albedo values for the sites were selected from Matthews (1984). While a satellite measurement of surface albedo was available from GOES visible channel data, it has been shown that this single green channel measurement systematically underestimates the albedos of most soils and vegetation and thus the Matthews values were deemed more suitable for model flux calculations. It is our intention in the near future to replace these albedos with values obtained from multispectral satellite information. Surface emissivity values were selected based on research by Kondrat'yev (1969), Fuchs and Tanner (1966), Taylor (1979) and Buettner and Kern (1965). The values of albedo and emissivity for the sites are also shown in Table 2.

5. Results

For each station location shown in Figure 3 and Table 2 an ensemble of MLM runs was made varying B_0 and Z_0 about the climatological means and using the site-specific 12 UTC atmospherics of 20 July 1981 in the model. Subsequently, a search/interpolation procedure was used to determine which model values of B_0 and Z_0 produced the measured values of DH and DT_s shown in Table 2. The results of this evaluation are also shown in Figure 3. The top number in light print in this figure shows the geographical location of the station with the numerical order (1-10) corresponding to the order of stations in Table 2. The number below

left of the station number is the Bowen ratio derived at the location, while the number below right is the roughness length in cm. As shown, the numbers appear quite reasonable and spatially coherent and depict well the sharp change in surface moisture and roughness which is known to take place across the central United States.

Figure 4 shows a selection of 12-hour model atmospheric simulations produced using the derived values of B_0 and Z_0 at some of the test locations going across the central United States, compared with radiosonde verification at 00 UTC 21 July. Since the 12 UTC atmospherics at these locations were the same ones used in the model to derive B_0 and Z_0, by definition in the methodology the height of the PBL must match the verification. We are encouraged though that the model prediction of atmospheric temperature in the mixed layer, which is unconstrained by the methodology, is also predicted quite well in these dependent sample tests.

As an independent test of the B_0,Z_0 results, the derived Bowen ratio and roughness values derived on 20 July were used in 12-hour MLM simulations at some of the station locations which were cloud free on the days of 22 July and 23 July 1981. Table 3 shows the accuracy statistics of these tests. The temperature and height of the mixed layer are predicted quite well, within 1.31 degrees C and 14.2 mb., respectively. On 22 July GOES-4 data was available to verify the model prediction of the diurnal skin temperature range. As shown in Table 3, this range is also reasonably well predicted in these MLM simulations, with an overall standard error of 2.48 degrees C.

Figures 5 and 6 each show four examples of 12-hour simulations produced in these independent tests, compared with radiosonde

verification. Figures 5a-5d show subjectively the "best" results going across moisture regimes wet to dry, while Figures 6a-6d are a similar display for the "worst" model results on 22 and 23 July. Perhaps the most encouraging feature in all these simulations is the good accuracy in the prediction of the mixed layer height across both "best" and "worst" examples. The most obvious flaw is in the consistent under-prediction of the mixed layer temperatures in the "worst" display, which can also be quite clearly seen in the results listed in Table 3. In these independent trials we were not as careful to screen the locations for the presence of advection, as was done on 20 July when the B_0 and Z_0 results were derived. Still, it seems unlikely that warm advection could be responsible in all these cases for the model under-prediction of temperature and it is more probable some atmospheric process which the model now neglects is responsible for the disparity. Considering that both the dependent and independent samples all represent conditions of clear skies, a strong possibility is that large scale subsidence is biasing the results and that an evaluation of this process for the MLM (for example from a 3-d model) would improve the basic findings of this study. This is now being investigated. It can be seen, however, that with the removal of this bias error that the prediction of mixed layer temperature shown in Table 3 would be greatly improved.

5. Error Evaluation

While it is clear that a larger ensemble of tests will be necessary to establish a good evaluation of the error characteristics of the DH,DT_s methodologies introduced in this work, it is possible at this point in time to make some preliminary remarks on this topic.

In evaluating B_0 and Z_0 from radiosonde and satellite data on 20 July, we have located the single values of these variables which produce the measured DH and DT_s in model simulations. In practice, however, there is a range of potential solutions for B_0 and Z_0 around these single values whose bounds are determined by modelling and measurement errors for DH and DT_s. Our preliminary investigations suggest that when surface forcing dominates the changes in the lower atmosphere, that total model and measurement accuracy in the surface temperature range is about 2 degrees C, while combined modelling and measurement accuracy for the height of the mixed layer is about 100 and 200 m, respectively, for wet and dry surface moisture regimes.

The shaded areas in Figure 2 show then "envelopes" of solutions for B_0 and Z_0 about a center location, all of which would be possible given these approximate error bounds. It is clear from these figures that errors in B_0 and Z_0 are situation dependent and will relate to the specific functional dependencies of DH and DT_s on B_0 and Z_0 for given atmosphere/surface set of conditions.

In Figure 2a, a wet and rough surface regime, the bounds of the solution envelope in B_0 and Z_0 are B_0 = .38 to .64 and Z_0 = 20.7 to 80.2 cm. The variation in B_0 for this period in mid July translates to an error of approximately 1.1 $MJ\text{-}m^{-2}$ in the evaluation of 12-hour surface sensible heating. In a surface energy balance scheme, the errors in the evaluation of surface latent heating from these methods would be approximately equal but of opposite sign. The 1.1 $MJ\text{-}m^{-2}$ figure can be compared to an approximate net solar radiation for this latitude and season of 22 $MJ\text{-}m^{-2}$.

Two similar solution envelopes are shown in Figure 2b for the dry and smoother surface regime. The upper envelope in this figure has a range of solutions about the center, given the estimated errors in DH and DT_s, of B_0 = 1.1 to 1.3 and Z_0 = 5.1 to 7.2 cm. Similar solution bounds for the envelope shown in the lower part of the figure are B_0 = 3.91 to 6.13 and Z_0 = .22 to 1.3 cm. These two ranges of Bowen ratio for the two envelopes translate to a magnitude of sensible/latent heating error over 12 hours of about .64 and .79 MJ-m^{-2}, respectively. Again, this can be compared to about 22 MJ-m^{-2} of available solar energy for this latitude and season. These preliminary accuracy results for dry and smooth locations are much better than the results shown in Table 1 for similar regimes, where the land surface turbulent fluxes have been evaluated from satellite-measured surface skin temperatures alone.

6. Conclusions

A simple method has been presented to evaluate effective land surface roughness and surface turbulent fluxes using measurements of the height change of the atmospheric PBL from radiosonde reports and geostationary satellite measurements of surface skin temperature range. The methods have been applied to assess the regional variation of fluxes and surface roughness across the sharp transition zone of surface climatology in the central United States. A preliminary error analysis indicates that expected errors in the evaluation of 12-hour sensible/latent heating from these methodologies are situation dependent but should be in the range of 1 MJ-m^{-2} across a large range of surface climatologies.

As with any new methodologies, there are potential caveats which will need to be investigated. Values of B_0 and Z_0 derived through these procedures will always to some extent be model specific. The sets of model runs which we have completed have yielded unique B_0 and Z_0 values for the measurement values of DH and DT_s. It is likely, however, that in other situations or when using more complex (and presumably more sophisticated) models of the surface, where the effective skin temperature depends on more subtle canopy and soil properties (leaf area index, biomass, etc.), that this may not be the case and that more detailed investigation will be necessary. It can be immediately seen, however, that as surface parameterizations grow more realistic and accurate so do the results of these DH,DT_s techniques. By definition the surface/PBL model used to derive B_0 and Z_0 will produce values of DH and DT_s at a location which correspond to measurements. For the example then of Z_0 in a simple surface model such as ours, this roughness height is then an "effective" value which produces the correct values of DH and DT_s. Consequently, we expect that many of the systematic deficiencies of simple models can be compensated for through this procedure. As model sophistication increases, or if other satellite of land use information can be applied, this "effective" surface roughness or other derived surface characteristic will converge towards a value with increased physical meaning.

For the present at least, the required combination of DH and DT_s signals is only available at radiosonde locations. While it is not true that surface roughness need be horizontally continuous, as is the case with atmospheric temperature, Z_0 does in general follow patterns of vegetation dictated by surface moisture climatology. Thus, the

roughness values produced at radiosonde sites may be suitable for objective analysis techniques, which could produce a more consistent estimate of Z_0 away from radiosonde locations. We would also expect that averaging independent assessments of Z_0 using our techniques on several days of data will produce more accurate values, since surface roughness is a quantity which changes relatively slowly with time.

One of the most exciting and useful prospects for these techniques for diagnosis of the surface energy balance and roughness will come with the launch of space-based lidar systems planned for the 1990's. The accuracy goal for the proposed Lidar Atmospheric Sounder and Altimeter (LASA) instrument is 50 m in the retrieval of the PBL height (Curran, 1987). Hopefully this lidar system will be beneficial in monitoring the smaller scales of surface conditions which cannot be resolved by the synoptic network.

ACKNOWLEDGMENTS

This work was supported under the NASA Interdisciplinary Satellite Land Surface Climatology Program (ISLSCP), grant NAG5-854.

REFERENCES

Buettner, K., and D. Kern, 1965: The determination of infrared emissivities of terrestrial surfaces. J. Geophys. Res., 70, 1329-1337.

Chou, S., and D. Atlas, 1982: Satellite estimates of ocean-air heat fluxes during cold air outbreaks. Mon. Wea. Rev., 110, 1434-1450.

Curran, R. J. (Ed.), 1987: LASA, Lidar Atmospheric Sounder and Altimeter. Earth Observ. Syst. Rep. IId, 91 pp., NASA.

Diak, G. R., and T. R. Stewart, 1989: Assessment of surface turbulent fluxes using geostationary satellite surface skin temperatures and a mixed layer planetary boundary layer scheme, Accepted for publication in J. Geophys. Res.

Diak, G. R., S. Heikkinen, and J. Bates, 1986: The influence of variations in surface treatment on 24-hour forecasts with a limited area model, including a comparison of modelled and satellite measured surface temperatures. Mon. Wea. Rev., 114, 215-232.

Driedonks, A. G. M., 1982a: Models and observations of the growth of the atmospheric boundary layer, Boundary Layer Meteorol., 23, 284-306.

Driedonks, A. G. M., 1982b: Sensitivity analysis of the equations for a convective mixed layer. Boundary Layer Meteorol., 22, 475-480.

Driedonks, A. G. M., and H. Tennekes, 1984: Entrainment effects in the well-mixed atmospheric boundary layer. Boundary Layer Meteorol., 30, 75-105.

Fuchs, M., and C. B. Tanner, 1966: Infrared thermometry of vegetation. Agron. J., 58, 239-253.

Kondrat'yev, K. P. A., 1969: Radiation in the Atmosphere, 859 pp., Academic, San Diego, CA.

Matthews, E., 1984: Prescription of land-surface boundary conditions in GISS GCM 11: A simple method based on high-resolution vegetation data bases, NASA Tech. Memo 86096, 20 pp., Goddard Space Flight Center, New York.

Peterson, R. A., D. Keyser, A. Mostek, and L. Uccellini, 1983: Severe storms analysis and forecasting techniques using VAS satellite data. Proc. 13th Conf. Severe Local Storms, Boston, MA, AMS, 375 pp.

Sellers, P. J., Y. Mintz, Y. C. Sud, and A. Dalcher, 1986: A simple biosphere model for use within general circulation models. J. Atmos. Sci., 43, 505-531.

Smith, W. L., V. E. Suomi, F. X. Zhong, and W. P. Menzel, 1982: Nowcasting applications of geostationary satellite atmospheric sounding data, in Nowcasting, pp. 123-135, Academic, San Diego, CA.

Taylor, E., 1979: Measured emissivity of soils in the southeast United States. Remote Sens. Environ., 8, 359-364.

Wetzel, P., D. Atlas, and R. Woodward, 1984: Determining soil moisture from geosynchronous satellite infrared data: A feasibility study. J. Clim. Appl. Meteorol., 23, 375-391.

Zilitinkevich, S. S., 1975: Comments on "A model for the dynamics of the inversion above a convective boundary layer." J. Atmos. Sci., 32, 991-992.

TABLE 1 Errors in Model-Predicated 12-hour Sensible Heating Resulting From Errors in Surface Temperature Measurement, Roughness Height Assignment, and Upper Boundary Conditions for Varying Evaporations and Roughness Regimes

	z_0, cm											
	1		5.7		11.6		20.1		31.9		48.1	
Bowen Ratio	εQ_0, MJ m^{-2}	$\varepsilon Q_0/SW_n$	εQ_0, MJ m^{-2}	$\varepsilon Q_0/SW_n$	εQ_0, MJ m^{-2}	$\varepsilon Q_0/SW_n$	εQ_0, MJ m^{-2}	$\varepsilon Q_0/SW_n$	εQ_0, MJ m^{-2}	$\varepsilon Q_0/SW_n$	εQ_0, MJ m^{-2}	$\varepsilon Q_0/SW_n$
0.3	1.87	0.08	1.31	0.06	1.31	0.06	0.92	0.04	0.73	0.03	0.72	0.03
0.4	1.84	0.08	1.43	0.06	1.38	0.06	1.32	0.06	1.25	0.05	0.93	0.04
0.5	2.30	0.10	1.94	0.08	1.70	0.07	1.15	0.05	1.13	0.05	1.01	0.04
1.0	3.47	0.15	2.60	0.11	2.07	0.09	1.91	0.08	1.70	0.07	1.20	0.05
2.0	4.40	0.19	3.23	0.14	2.77	0.12	2.73	0.12	2.31	0.10	1.62	0.08
3.0	5.01	0.22	3.72	0.16	3.24	0.14	3.21	0.14	2.60	0.11	2.07	0.09
10.0	6.43	0.28	3.91	0.17	3.69	0.16	3.66	0.16	3.00	0.13	2.51	0.11
1000	6.68	0.29	4.15	0.18	3.91	0.17	3.89	0.17	3.24	0.14	2.77	0.12

Here εQ_0 is the standard sensible heating error, while $\varepsilon Q_0/SW_n$ is the same error normalized to a 12-hour net shortwave flux total of 22 MJ m^{-2}.

TABLE 2

Synoptic stations used for B_0 and Z_0 evaluation

Station	Character	A(%)	ϵ	DH(m)	DT_s(°C)
247	Wet	19	.98	1192	6.5
229	Wet	18	.98	1899	6.5
311	Wet	18	.98	1977	6.5
260	Intermediate	19	.96	1658	14.0
261	Intermediate	20	.96	1607	14.5
363	Intermediate	19	.96	3659	20.6
365	Dry	17	.94	3124	30.5
486	Dry	20	.94	3827	30.5
476	Dry	18	.94	3863	28.0
576	Dry	18	.94	3767	28.5

Shown for each synoptic location are the surface moisture character, the albedo, A, the surface emissivity, ϵ, and the measurement values of DH and DT_s.

TABLE 3

Errors in Independent Trials (Models Versus Radiosonde and Satellite Measurements) for Model-Predicted Mixed Layer Quantities

	STN	$\overline{\Delta T}$ (°C)	$\lvert\Delta H\rvert$ (mbar)	T_{SM} (°C)	T_{SP} (°C)	DT_S (°C)	B_0	Z_0 (cm)
22 July	247	-1.6	15	5.5	6.7	1.2	.33	32
	229	-1.8	5	8.5	6.2	-2.3	.45	49
	260	-.4	7	11.5	15.5	4.0	.90	1.0
	261	-1.8	10	16.0	17.9	1.9	.79	1.7
	365	.6	12	35.5	29.9	5.6	4.2	1.3
	486	-.3	*	32.5	32.6	.1	650	1.3
	476	-3.0	4	33.5	30.4	3.1	500	1.0
	576	.3	*	31.0	29.4	-1.6	1000	1.2
23 July	247	-2.2	30	-	-	-	.33	32
	365	-1.5	22	-	-	-	4.2	1.3
	486	.9	23	-	-	-	650	1.3

$\sigma\Delta T$=1.31 $\sigma\lvert H\rvert$=14.2 $\sigma\Delta T_S$=2.48

Shown for synoptic stations are errors in 12 hour prediction of mixed layer air temperature, $\overline{\Delta T}$, mixed layers height, $\lvert\Delta H\rvert$, measured and model-preidcted diurnal surface skin temperature range, T_{SM} and T_{SP}, and the difference between these two quantities, ΔT_S. B_0 and Z_0 are the derived Bowen ratio and surface roughness which have been utilized in the model prediction. Standard errors in the surface temperature range, $\sigma\Delta T$, and height of the mixed layer, $\sigma\lvert H\rvert$, are also shown.

*indicates distinct mixed layer verification height not readily discernible

FIGURE CAPTIONS

Fig. 1 Schematic representation of hybrid mixed layer/surface layer model.

Fig. 2. Dependence of 12-hour surface skin temperature range (°C, solid lines) and rise of the mixed layer height (m, dashed lines) on surface roughness (cm) and Bowen ratio (dimensionless) from MLM simulations. Figure 2A is for a wet and rough climatological region, while 2B is for a drier and smoother surface climatology. Shaded areas depict range of possible B_0 and Z_0 values for estimated modelling and measurement errors in the PBL height and surface skin temperature range.

Fig. 3. Synoptic stations selected for evaluation of Bowen ratio and surface roughness. The number in light type shows the synoptic station location with the numerical order (1-10) following the order of stations listed in Table 2. The number to the lower right of the station number is the evaluated roughness height (cm) while the number to the lower left is the measured Bowen ratio (dimensionless).

Fig. 4. Skew T - log p diagrams of temperature and dewpoint temperature (°C) from 12-hour MLM simulations employing derived values of B_0 and Z_0 on 20 July 1981. Heavy and light lines are model simulation and radiosonde verification, respectively. Synoptic station order of panels A through D is 247, 261, 363, and 486.

Fig. 5. Skew T - log p diagrams of temperature and dewpoint temperature (°C) from "best" 12-hour forecasts on 23 and 24 July 1981 versus radiosonde verification. Synoptic station order of panels A through D is 260, 365, 365, and 486.

Fig. 6. Same as Fig. 5, only "worst" results. Synoptic station order of panels A through D is 247, 229, 261, and 476.

APPENDIX A

List of Symbols for Figure 1

γ_θ, γ_U, γ_V, γ_q	Vertical gradients of temperature, U and V winds, and specific humidity above the mixed layer.
H	Height of mixed layer.
$\overline{W}$	Vertical velocity at mixed layer height.
A_F, A_T	Scaling constants.
g	Gravitational acceleration.
T_o	Scaling temperature.
σ_w	Scaling velocity for vertical component of turbulent kinetic energy.
$\Delta\theta$, ΔU, ΔV, Δq	"Jumps" of potential temperature, U and V wind components and specific humidity at the top of the mixed layer.
θ_m, U_m, V_m, q_m	Mean mixed layer values of potential temperature, U and V wind components, and specific humidity.
Z_c	Constant flux layer height.
Z_0	Surface roughness.
$\overline{\theta W}_s$, $\overline{UW}_s$, $\overline{VW}_s$, $\overline{qW}_s$	Surface layer turbulent fluxes of potential temperature, U and V momentum, and specific humidity.
θ_*, U_*, q_*	Surface layer scaling potential temperature, wind velocity, and specific humidity.
S_0	Incident solar flux at surface.
A	Surface albedo.
ϵ	Surface emissivity.
σ	Stefan-Boltzmann constant.
T_s	Surface skin temperature.
$LW\downarrow$	Atmospheric longwave flux to surface.
G_0	Submedium flux.
Z	Vertical distance below surface

C	Soil heat capacity.
K	Soil conductivity.
T	Subsoil temperature.
t	Time.

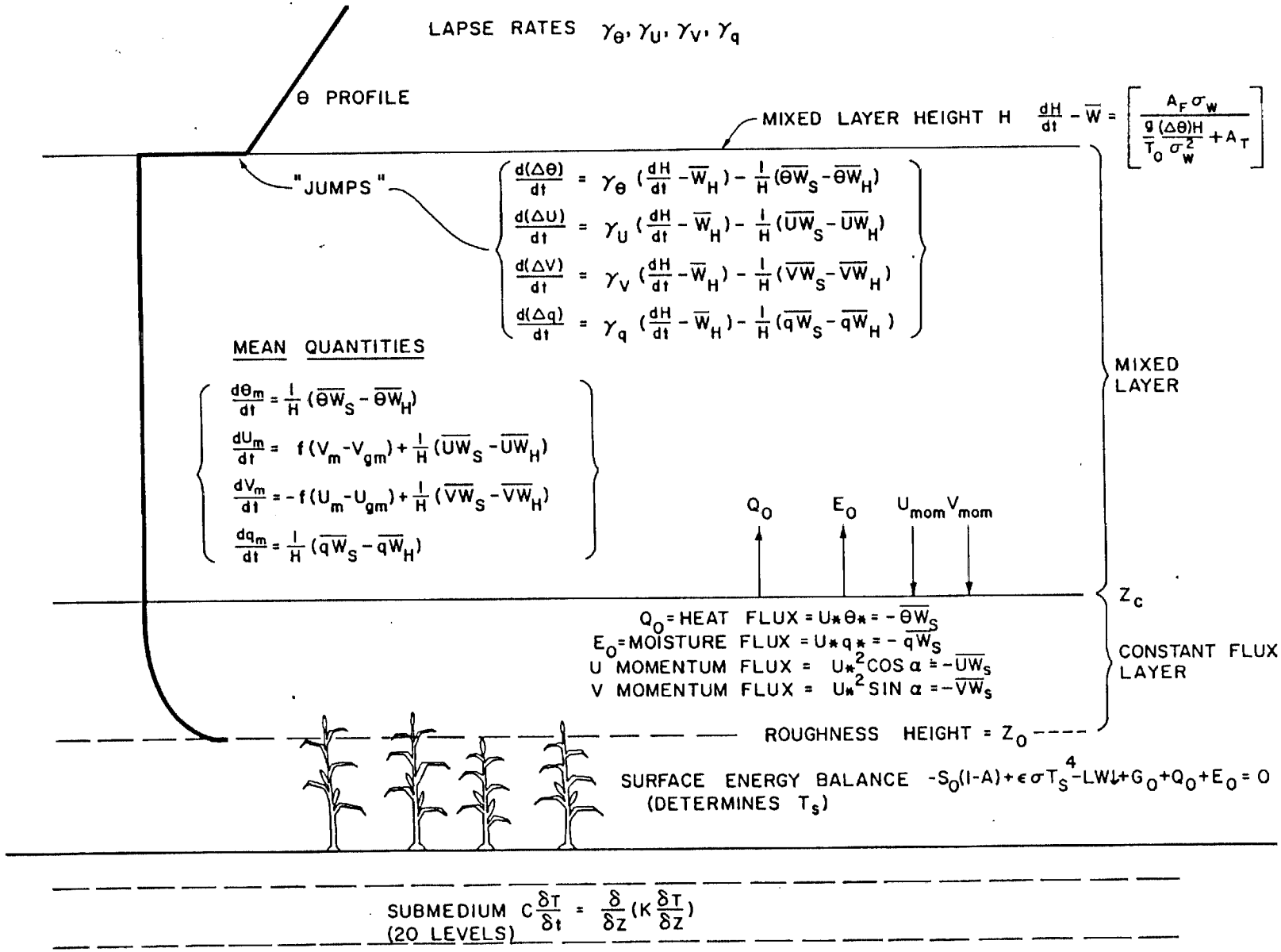
LAPSE RATES $\gamma_\theta, \gamma_U, \gamma_V, \gamma_q$
θ PROFILE
MIXED LAYER HEIGHT H
$\frac{dH}{dt} - \overline{W} = \left[\frac{A_F \sigma_w}{\frac{g(\Delta\theta)H}{T_0 \sigma_w^2} + A_T}\right]$
"JUMPS"
$\frac{d(\Delta\theta)}{dt} = \gamma_\theta \left(\frac{dH}{dt} - \overline{W}_H\right) - \frac{1}{H}(\overline{\theta W}_S - \overline{\theta W}_H)$
$\frac{d(\Delta U)}{dt} = \gamma_U \left(\frac{dH}{dt} - \overline{W}_H\right) - \frac{1}{H}(\overline{UW}_S - \overline{UW}_H)$
$\frac{d(\Delta V)}{dt} = \gamma_V \left(\frac{dH}{dt} - \overline{W}_H\right) - \frac{1}{H}(\overline{VW}_S - \overline{VW}_H)$
$\frac{d(\Delta q)}{dt} = \gamma_q \left(\frac{dH}{dt} - \overline{W}_H\right) - \frac{1}{H}(\overline{qW}_S - \overline{qW}_H)$
MEAN QUANTITIES
$\frac{d\theta_m}{dt} = \frac{1}{H}(\overline{\theta W}_S - \overline{\theta W}_H)$
$\frac{dU_m}{dt} = f(V_m - V_{gm}) + \frac{1}{H}(\overline{UW}_S - \overline{UW}_H)$
$\frac{dV_m}{dt} = -f(U_m - U_{gm}) + \frac{1}{H}(\overline{VW}_S - \overline{VW}_H)$
$\frac{dq_m}{dt} = \frac{1}{H}(\overline{qW}_S - \overline{qW}_H)$
MIXED LAYER
Q_0 E_0 U_{mom} V_{mom}
Z_c
Q_0 = HEAT FLUX = $U_* \theta_* = -\overline{\theta W}_S$
E_0 = MOISTURE FLUX = $U_* q_* = -\overline{qW}_S$
U MOMENTUM FLUX = $U_*^2 \cos\alpha = -\overline{UW}_S$
V MOMENTUM FLUX = $U_*^2 \sin\alpha = -\overline{VW}_S$
CONSTANT FLUX LAYER
ROUGHNESS HEIGHT = Z_0
SURFACE ENERGY BALANCE $-S_0(1-A) + \epsilon\sigma T_S^4 - LW\downarrow + G_0 + Q_0 + E_0 = 0$
(DETERMINES T_s)
SUBMEDIUM (20 LEVELS) $C\frac{\delta T}{\delta t} = \frac{\delta}{\delta Z}(K\frac{\delta T}{\delta Z})$

Figure 1

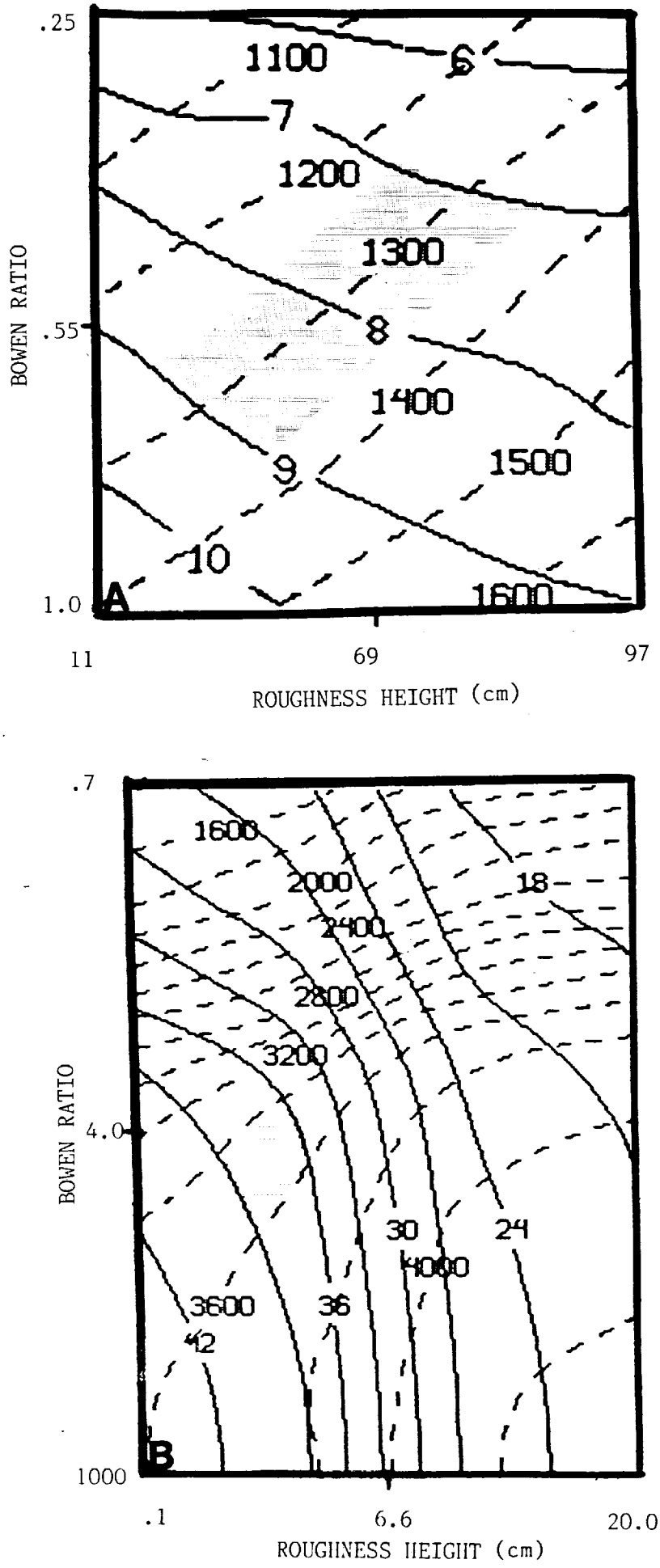
.25
1100
6
7
1200
1300
8
1400
9
1500
10
1600
A
1.0
BOWEN RATIO
.55
11
69
97
ROUGHNESS HEIGHT (cm)
.7
1600
2000
18
2400
2800
3200
4.0
BOWEN RATIO
30
24
4000
3600
36
42
B
1000
.1
6.6
20.0
ROUGHNESS HEIGHT (cm)

Figure 2

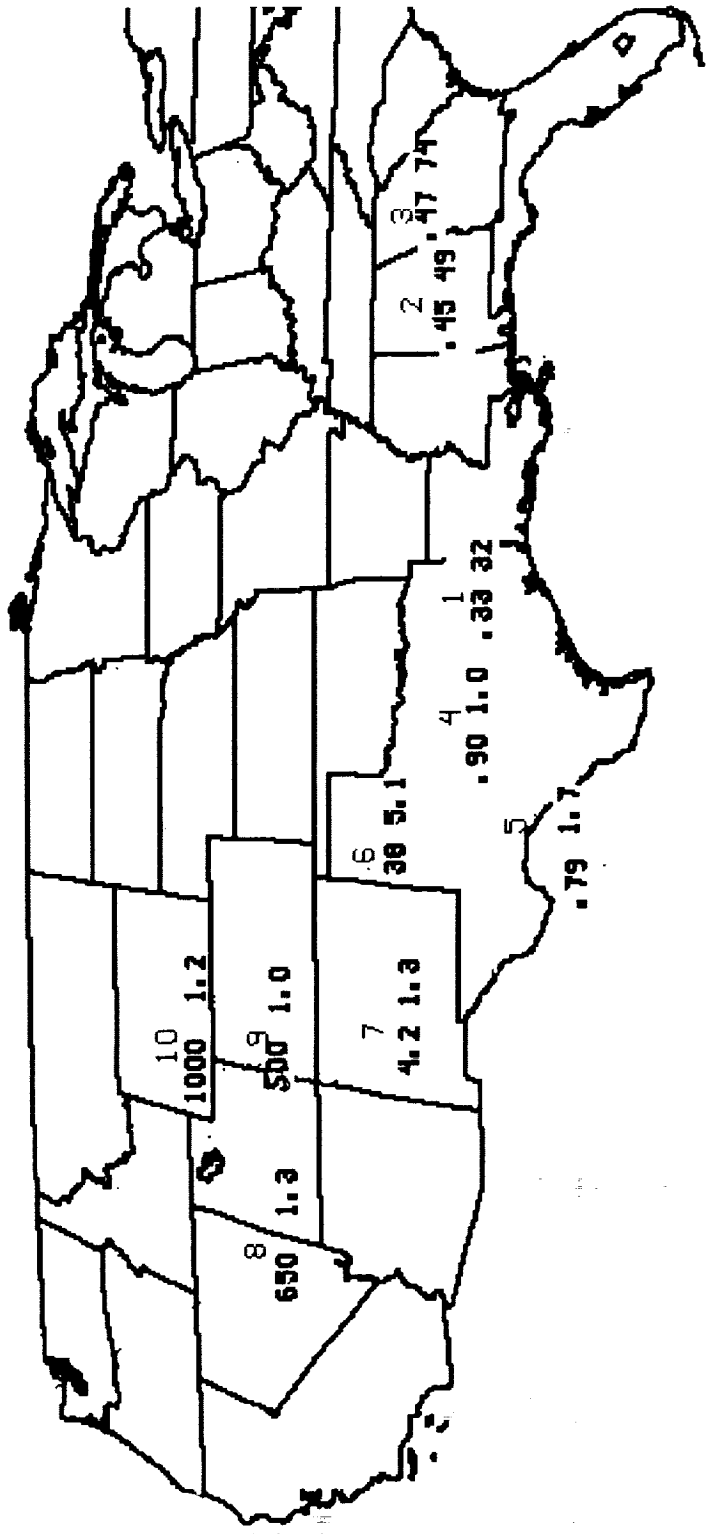
3 .47 74
2 .45 49
1 .33 32
4 .90 1.0
5 .79 1.7
6 38 5.1
7 4.2 1.3
9 500 1.0
10 1000 1.2
8 650 1.3

Figure 3

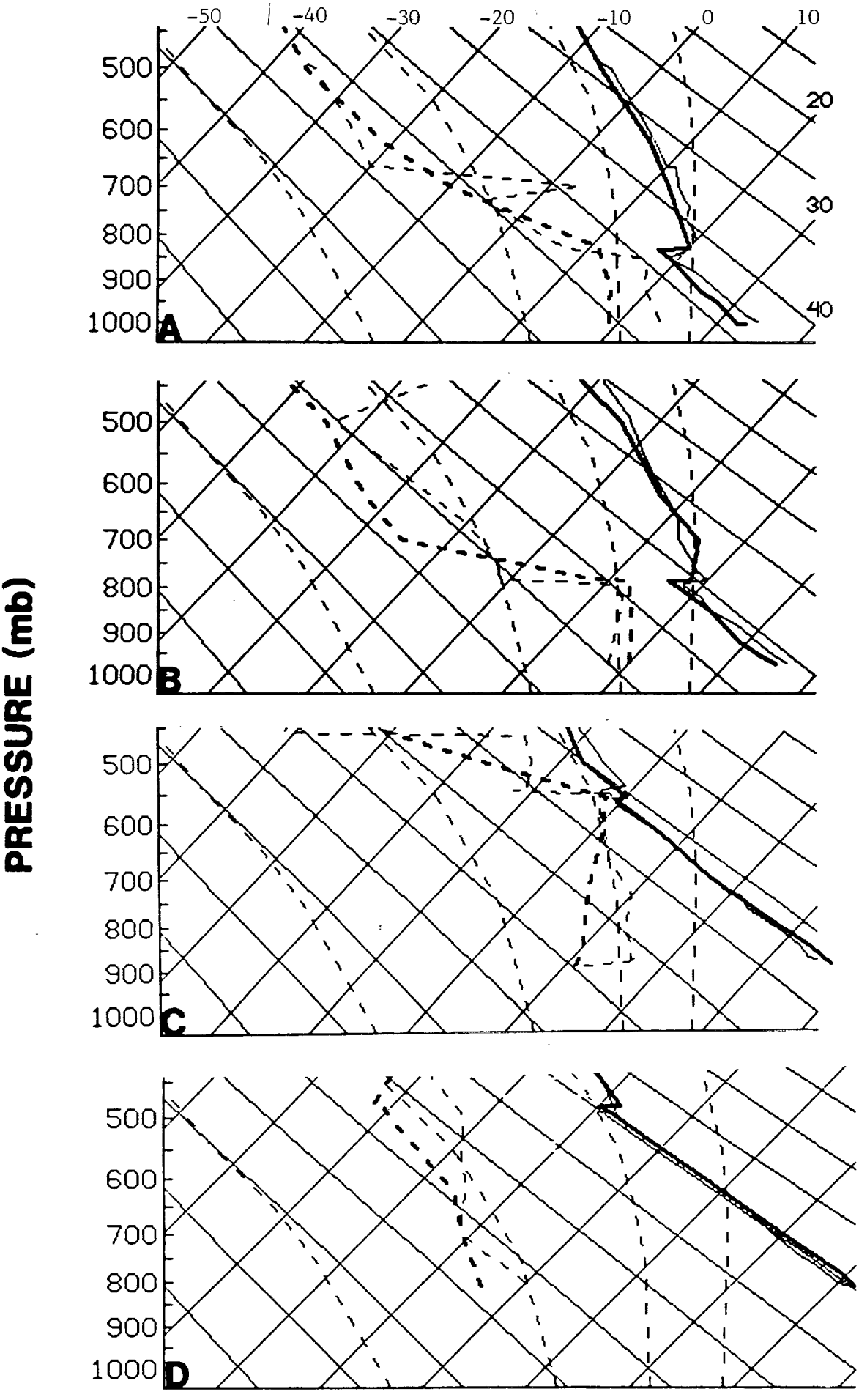
-50
-40
-30
-20
-10
0
10
500
600
700
800
900
1000
20
30
40
A
B
C
D
PRESSURE (mb)
TEMPERATURE (°C)

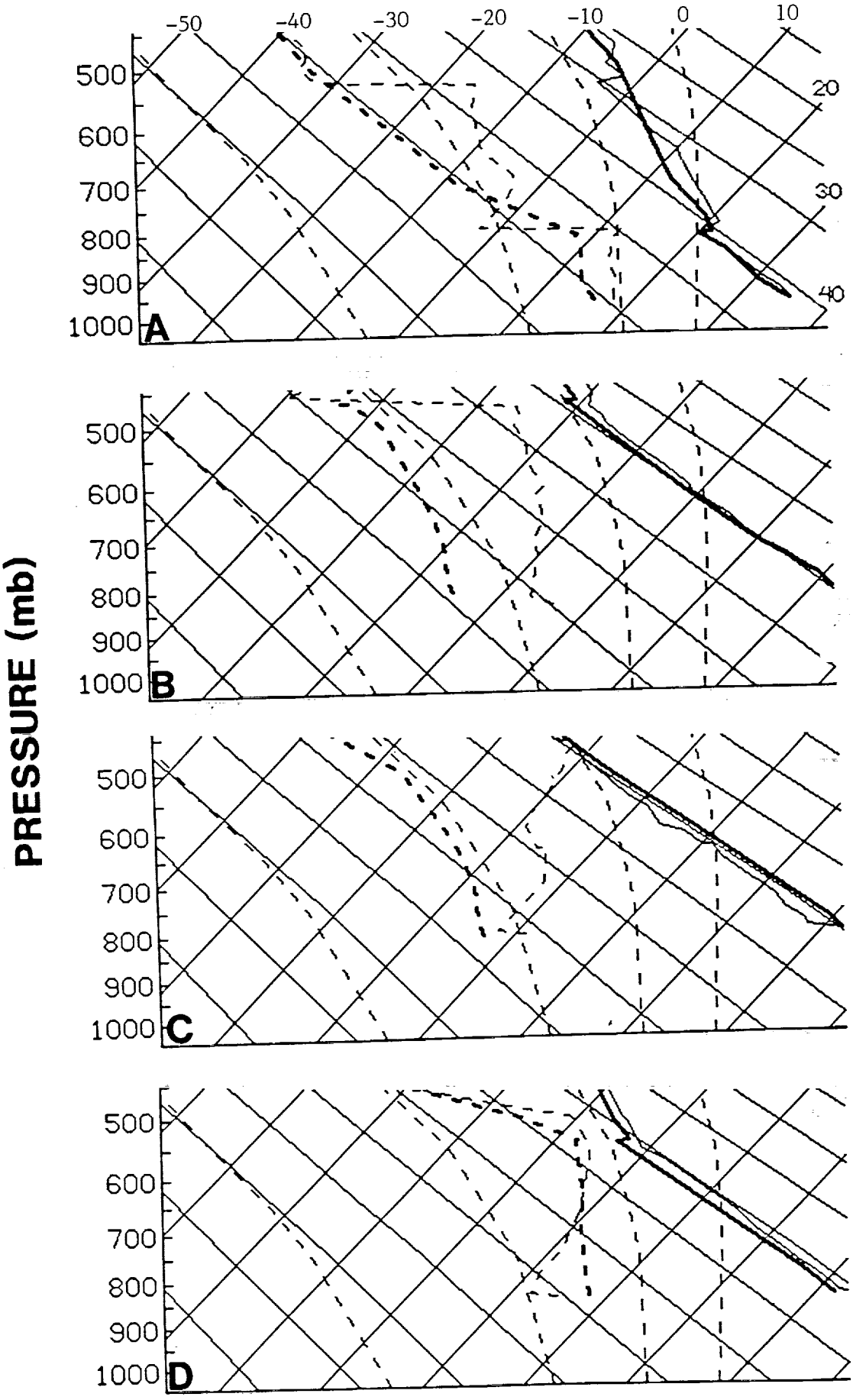
-50
-40
-30
-20
-10
0
10
20
30
40
500
600
700
800
900
1000
A
B
C
D
PRESSURE (mb)
TEMPERATURE (°C)

Figure 5

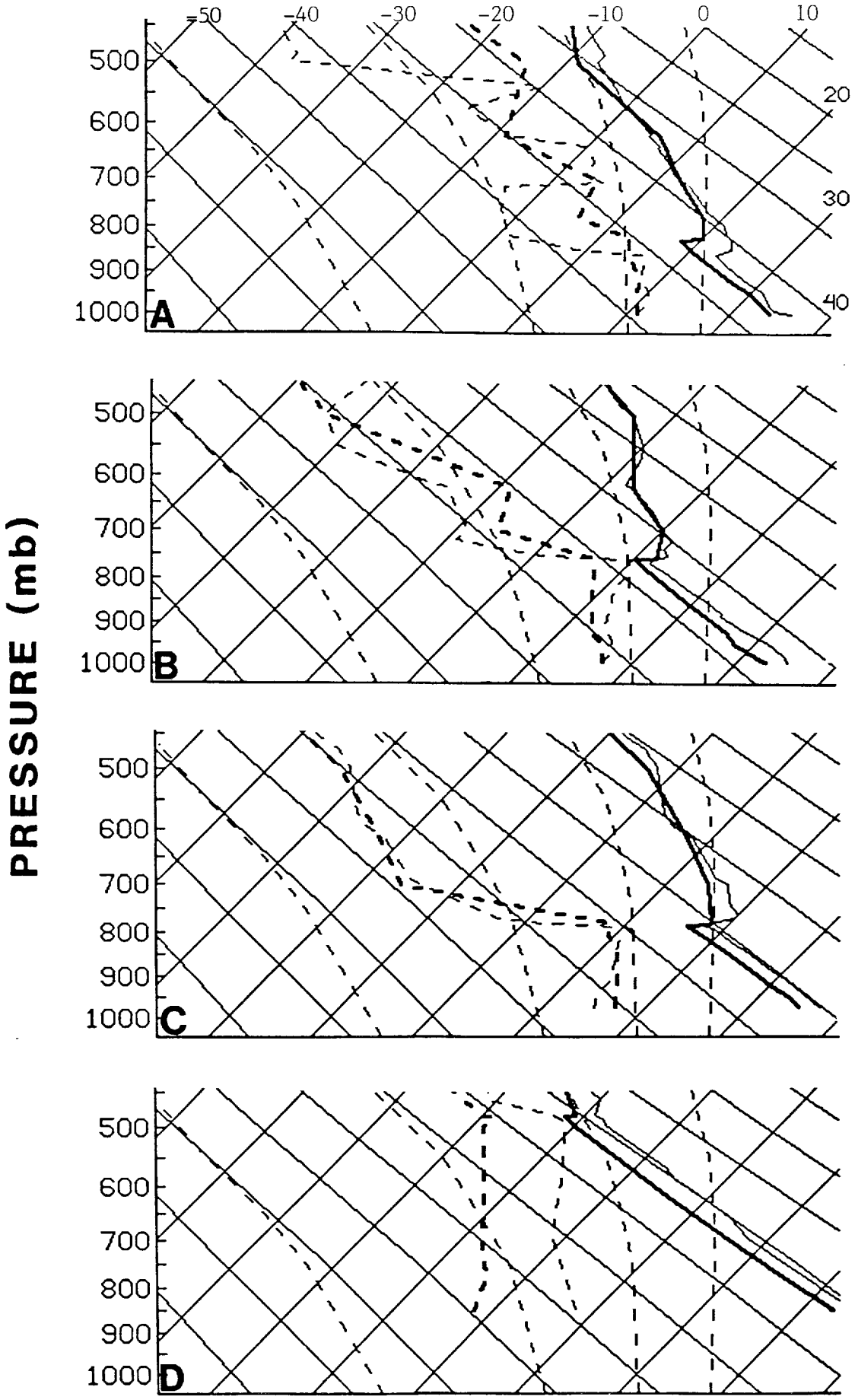
-50
-40
-30
-20
-10
0
10
20
30
40
500
600
700
800
900
1000
A
B
C
D
PRESSURE (mb)
TEMPERATURE (°C)

Figure 6

The Utility Of The High Resolution Interferometer Sounder In The Remote Sensing Of Land Surface Energetics And Planetary Boundary Layer Development

by

Christopher John Scheuer

A thesis submitted in partial fulfillment of the requirements for the degree of

Master Of Science

(Meteorology)

at the

UNIVERSITY OF WISCONSIN-MADISON

1989

Abstract

Three versions of an atmospheric and land-surface radiance signal algorithm are developed in an attempt to remotely evaluate the land-Surface Energy Budget (SEB). The characteristics of the radiances are based on the High Resolution Interferometer Sounder (HIS). A composite surface-mixed layer atmosphere model is used to generate a set of atmospheres which have been modified by energy exchanges with the land-surface. Synthetic radiances for the model output and initialization atmospheres are calculated and then differenced to recover a radiance change or signal. Results with a dependent data set reveal that correlations of better than 0.90 between SEB terms and eigenvector coefficients evaluated from the radiance signals are achievable. However, these accuracies appear to be highly dependent on both the length of the model time integration and the amount of land-surface moisture. A study on the applicability of the methods developed in this work to real atmospheric data shows that the predicted SEB values based on 12 hour atmospheric radiance changes synthesized from Radiosonde observations agree well with model calculations.

1. Introduction

This work is an investigation of the utility of the High Resolution Interferometer Sounder (HIS) instrument for observing the land-Surface Energy Budget (SEB). Remote evaluation of the SEB has been a goal in the research community for some time. Within the last decade, several approaches have been developed for the remote sensing of the SEB and/or soil moisture. Satellite-measured infrared land surface temperatures have been used in several studies [Diak and Stewart, 1989, Wetzel et al., 1984, Carlson et al., 1981] to infer the surface turbulent flux balance and soil moisture. Also, microwave techniques (Schmugge, 1987) have the potential to allow direct measurement of surface moisture via the dependence of surface emissivity on surface moisture.

An improved understanding of the SEB will have several meteorological applications. Evapotranspiration anomalies produced by soil moisture anomalies can be important to model simulated climatologies (Sud and Fennessy, 1984). A study by Garret (1982) on mesoscale circulations showed that the vegetative cover, the soil moisture, and the roughness affect the location of convective cells via the

development of the Planetary Boundary Layer (PBL). Accurate surface flux predictions may be important for useful prediction of synoptic and mesoscale events (Diak et al., 1986). Land-surface energy budget considerations must also be accounted for in the study of the general circulation. Energy exchanges between the surface and the free atmosphere occur in the PBL through penetrative convection or through the temporal variations in the PBL depth (Suarez et al., 1983). These considerations led to the inclusion of the PBL depth as a prognostic variable in the University of California at Los Angeles general circulation model.

Early efforts to remotely sense the surface turbulent flux balance relied on the measurement of the absolute land-surface temperature. An evaluation of the vertical gradient of surface air temperature is inherent in these models, which is then used to establish surface sensible heating. Air temperatures were evaluated at anemometer height (approximately 2 meters). Inaccuracies in specifying this gradient over such a small vertical extent introduced large errors in the flux calculations. More recent attempts have attempted to eliminate this problem by (1) using land-surface temperature changes rather than

the absolute temperature to eliminate errors introduced by sensor calibration, errors in the land-surface emissivity, and atmospheric attenuation effects and (2) reducing the surface-air temperature gradient errors by calculating this gradient over a larger vertical interval through the use of a planetary boundary layer model.

In the work presented here, changes in upwelling radiance are used to infer lower tropospheric changes resulting from energy input into the lower atmosphere from the surface. The radiances are based on the spectral resolution of the High Resolution Interferometer Sounder (HIS) (Smith et. al, 1983). The ability of the HIS to resolve lower troposphere temperature and moisture excursions resulting from the surface forcings is of primary importance in this research. The HIS offers spectral and vertical resolution superior to that of the current generation atmospheric sounding system (Smith et. al, 1989). These features are highly desirable when attempting to resolve perturbations only 1-2 kilometers in depth, as is often the case with surface-induced PBL changes. This suggests that the HIS is a valuable instrument for studies of surface energetics and PBL development.

For the first time in this work, an attempt is made to quantify the SEB in terms of a remotely sensed radiance change originating from surface induced changes to the lower atmosphere. Previous SEB remote sensing efforts for the most part have used surface temperature excursions for this purpose.

In this study, a planetary boundary layer model is employed to generate a set of atmospheric profiles where the lower to mid troposphere is modified by surface forcings representing a variety of SEB conditions. There are two principal reasons why model data, rather than real atmospheric data are used. First, all input energy (i.e. solar heating) to the model is accounted for through a redistribution to the surface-atmosphere system. Second, this work requires accurate tabulations of the SEB and lower tropospheric changes over a large range of SEB conditions. Such a data set which is much easier to compile via simulation than through actual measurements.

The model is initialized with morning radiosonde reports from locations where advections can be assumed small, based on knowledge of the synoptic situation. When advections and shear-induced mixing are negligible, time changes in PBL quantities are dominated during these

daytime conditions by surface forcings. With this assumption, changes in upwelling radiance measured at the top of the atmosphere may be used to quantify surface-induced changes in the PBL.

HIS transmittances for the model initialization and output are calculated using a regression scheme based on the line-by-line FASCODE transmittance database (Clough et. al, 1986) with 20 mb. vertical resolution in the PBL. HIS radiances are derived through numerical integration of the radiative transfer equation (RTE). Three different radiance signatures are investigated. The first two are based on 12 and 8 hour PBL model integration intervals and include only the atmospheric term of the RTE. The third is based on an eight hour PBL model run and includes both the surface and atmospheric term in the RTE.

Eigenvector analyses on the simulated HIS radiances (Smith and Woolf, 1976) are then performed. The eigenvector coefficients are then included with several model diagnostics in a regression and correlation analysis. The purpose of the analysis is to provide insight via the spectral radiance change measured by HIS as to how the various surface forcings relate to the warming of the skin surface and the restructuring of the lower troposphere.

It is important to note that this research was done in a synthetic, controlled, and somewhat optimal environment. The last section of this work attempts to apply the results of this simulation study to actual atmospheric data (RAOB data). The results possible with actual satellite data may be compromised due to the influence of clouds, aerosols, and non-unity surface emissivity effects not considered here.

Table 5 Energy Terms Investigated (all energy terms in megajoules per meter squared)

$MJ\text{-}m^{-2}$

Range of values for 12 hours are listed above those for 8 hour runs

	Term	Definition	Range of Values
1)	Q_o	sensible heat flux;	4-13 2-6
2)	E_o	latent heat flux ;	0-13 0-7
3)	SW_n	$S_o(1-A)$;net shortwave flux;	19-22 8-13
4)	ΔH	diurnal PBL height excursion;	900-3900 m. 500-1900 m.
5)	G_o	submedium heat flux;	1-3 1-2
6)	Q_o/SW_n	ratio of sensible heat flux to net shortwave flux;	0.2-0.6 0.2-0.5
7)	E_o/SW_n	ratio of latent heat flux to net shortwave flux;	0.0-0.6 0.0-0.6
8)	$\Delta H/SW_n$	ratio of height excursion to net shortwave flux;	60-230 $m^3\text{-}MJ^{-1}$ 40-200 $m^3\text{-}MJ^{-1}$
9)	G_o/SW_n	ratio of submedium flux to net shortwave flux;	0.1-0.15 0.1-0.2

Table 6 Regression Statistics for the 12 Hour Atmospheric Radiance Signal

Quantity	σ_y	σ_e	s^2	R
Q_o	3.20	1.10	0.88	0.94
E_o	4.50	1.60	0.88	0.94
SW_n	0.80	0.50	0.52	0.73
ΔH	854.00	347.30	0.83	0.91
G_o	0.40	0.20	0.83	0.91
Q_o/SW_n	0.20	0.10	0.87	0.93
E_o/SW_n	0.20	0.10	0.88	0.94
$\Delta H/SW_n$	43.80	17.90	0.83	0.91
G_o/SW_n	0.02	0.01	0.83	0.90

where:

σ_y = standard deviation of the quantity;
σ_e = standard error of the estimate of quantity;
s^2 = the percent of variance in the term that is explained by the regression. (=1.0 for a perfect linear fit to the data)
R = the correlation coefficient of the regression (square root s^2), measure of the degree of linear association between quantity and the eigenvector coefficients. (=1.0 for a perfect linear fit)

Table 11 RAOB 72235 Retrieved Versus Model-Calculated SEB Terms

All energy terms in Megajoules/meter squared

Quantity	Retrieval	Model-Calculated	
Q_o	7.14	6.10	
E_o	8.07	9.98	
SW_n	21.16	21.59	
ΔH	1644 meters	1494 meters	(1411 meters)
G_o	2.06	1.82	

Table 12 RAOB 72365 Retrieved Versus Model-Calculated SEB Terms

All energy terms in Megajoules/meter squared

Quantity	Retrieval	Model-Calculated	
Q_o	11.16	13.15	
E_o	2.26	0.01	
SW_n	20.70	21.09	
ΔH	2578 meters	3267 meters	(3194 meters)
G_o	2.64	2.96	

Table 13 RAOB 72261 Retrieved Versus Model-Calculated SEB Terms

All energy terms in Megajoules/meter squared

Quantity	Retrieval	Model-Calculated	
Q_o	8.62	10.39	
E_o	5.92	3.50	
SW_n	20.89	20.47	
ΔH	2095 meters	1747 meters	(1221 meters)
G_o	2.23	2.44	

** Note: ΔH values in parentheses are verifications based on analyses of the RAOB data.